

Dissertation

submitted to the Combined Faculties
for the Natural Sciences and for Mathematics
of the Ruperto-Carola University of Heidelberg, Germany
for the degree of Doctor of Natural Sciences

presented by

Dipl.-Phys. **Justus Fuesers**

born in Solingen, Germany

Oral examination: 12th August 2013

Cell cycle correlations in epithelial tissue morphogenesis

Referees:

Dr. Stefano De Renzis

Prof. Dr. Ulrich Schwarz

Abstract

Epithelial organisation and integrity are crucial for the compartmentalisation of an organism and its organs and the regulation of information and energy flow. During early tissue morphogenesis, epithelial cells undergo a transition from a very dynamic and highly proliferative mesenchymal-like state to an immotile quiescent epithelial state. During this process cellular polarity changes from rear-front to apical-basal; a process essential for epithelial function.

We are interested in the origin of cell cycle correlations during this process and in the mechanism leading to their desynchronisation. We therefore quantify cell cycle correlations on the tissue level over several generations both *in vitro* and *in silico*. Furthermore, we consider their impact on cell migration during tissue morphogenesis. We use Madin-Darby Canine Kidney (MDCK-2) cells as an *in vitro* model for epithelial tissue morphogenesis and study cell cycle dynamics and cell migration by fluorescence time-lapse microscopy, automated image analysis, and single cell tracking.

We determine the narrow distribution of cell cycle periods at low cell density as the cause of the cell cycle correlations. A progressive desynchronisation occurs with each generation of cell divisions. At higher cell density, the desynchronisation process is further accelerated by contact inhibition of proliferation (CIP), resulting in a broadening of the cell cycle period distribution. We suggest that this growth control mechanism ensures the establishment and homeostasis of the emergent epithelial monolayer. Furthermore, we describe a mathematical model for free proliferation at low cell density. Our model confirms the origin of the cell cycle correlations and their progressive desynchronisation and predicts a stationary cell age distribution in case of unlimited growth. Finally, we quantify patterns of cell migration. We observe collective rotations of cell colonies at low cell density and find that changes in this behaviour correlate with mitoses. On the tissue level, synchronous cell divisions therefore involve perturbations of collective migration.

Taken together, we conclude that cell cycle correlations in epithelial tissue development are a transient phenomenon and that cells progressively desynchronise by two independent mechanisms, one of stochastic nature, the other one due to contact inhibition of proliferation. *In vitro*, synchronous cell divisions during early tissue morphogenesis are capable of disturbing tissue morphodynamics, in particular the patterns of collective migration.

Zusammenfassung

Die Integrität von Epithelien ist von essentieller Bedeutung für die Kompartimentalisierung von Organismen und ihren Organen, sowie die Regulierung von Informations- und Energietransport. Während der frühen Gewebemorphogenese gehen Epithelzellen von einem sehr dynamischen und proliferativen Verhalten über zu einem ruhenden epithelischen Gewebe. Im Zuge dessen ändert sich die für das Funktionieren des Epithels grundlegende zelluläre Architektur: So besteht anfangs eine Polarität zwischen hinteren und vorderen, später zwischen apikalen und basalen Pol.

Während dieses Übergangs verlaufen Zellzyklen über mehrere Generationen synchron zueinander. Im Rahmen dieser Arbeit untersuchen wir den Ursprung dieser Zellzykluskorrelationen und den Mechanismus der darauffolgenden Desynchronisierung, sowie deren Auswirkung auf die Zellmigration. Dazu quantifizieren wir die Zellzykluskorrelationen auf der Gewebeebene sowohl *in vitro* als auch *in silico*. Lebende Madin-Darby Canine Kidney (MDCK-2) Zellen dienen als *in vitro* Modell für die Morphogenese eines Epithels. Wir untersuchen die Dynamik von Zellzyklen und Zellmigration mittels Fluoreszenzmikroskopie, automatisierter Bildanalyse und dem Verfolgen einzelner Zellen über ihre gesamte Lebensdauer.

Als Ursache der Zellzykluskorrelationen ermitteln wir die schmale Verteilung der Zellzyklusdauern. Mit jeder Generation von Zellteilungen findet eine progressive Desynchronisierung statt. Bei höherer Zelldichte wird die Desynchronisierung durch das Auftreten der Kontaktinhibition der Proliferierung beschleunigt, indem sie zu einer Verbreiterung der Verteilung der Zellzyklusdauern führt. Wir legen nahe, dass dieser Wachstumskontrollmechanismus die Entstehung und Homöostase der emergenten epithelialen Zellmonoschicht fördert. Zusätzlich entwickeln wir ein mathematisches Modell, das die freie Zellproliferation bei niedriger Zelldichte beschreibt und den Ursprung der Zellzykluskorrelationen sowie ihre progressive Desynchronisierung bestätigt. Es sagt außerdem eine stationäre Altersverteilung im Falle uneingeschränkten Wachstums voraus. Schließlich quantifizieren wir auftretende Muster im Migrationsverhalten der Zellen. Bei niedriger Zelldichte beobachten wir kollektive Rotationen und dass Änderungen dieses Verhaltens mit Mitosen korrelieren.

Zusammenfassend stellen wir fest, dass Zellzykluskorrelationen in der Morphogenese von Epithelgewebe nur vorübergehend auftreten und durch zwei unabhängige Mechanismen aufgehoben werden: Die stochastische Verbreiterung der Generationen einerseits und die Auswirkungen der Kontaktinhibition bei hohen Zelldichten andererseits. Außerdem zeigt sich, dass synchrone Zellteilungen während der frühen Morphogenese Einfluss auf die Muster kollektiver Zellmigration nehmen.

Contents

Abstract	5
Zusammenfassung	7
Contents	9
Preface	11
1. Introduction	13
1.1. Epithelial tissues	13
1.2. Cell line model MDCK-2	17
1.3. Proliferation	19
1.4. Motility	27
1.5. Computational models	31
1.6. Thesis	35
2. Mitosis patterns in epithelial tissue growth	37
2.1. Colony growth	37
2.2. Cell cycle correlations	39
2.3. Model for free proliferation	40
2.4. Cell cycle heterogeneities	42
2.5. Conclusion	44
3. Migration and proliferation	45
3.1. Growth and motility dynamics	45
3.2. Migration patterns of young colonies	46
3.3. Dissecting changes in direction	48
3.4. Conclusion	49

4. Summary & Discussion	51
5. Materials & Methods	55
A. Appendix	59
A.1. Medium sensitivity	59
A.2. Density fluctuations	60
A.3. Spatially constrained tissues	61
Bibliography	63
List of Figures	73
Nomenclature	75
Acknowledgments	77

Preface

In this chapter I aim to give a personal view on the nature of biological systems by revealing several concepts and studies concerning the reductionism-holism debate in biology [Mazzocchi (2012)].

Wondering about the origins of life, Walker & Davies (2013) analysed the causal structure of living systems. They propose that the emergence of downward causation, i.e. the fact that in complex systems entities on hierarchically higher levels of organisation can determine the dynamics on lower levels, was a useful milestone by which living systems could be distinguished from non-living ones. Campbell had pointed out earlier that this concept is relevant in biology [in Ayala & Dobzhansky (1974)].

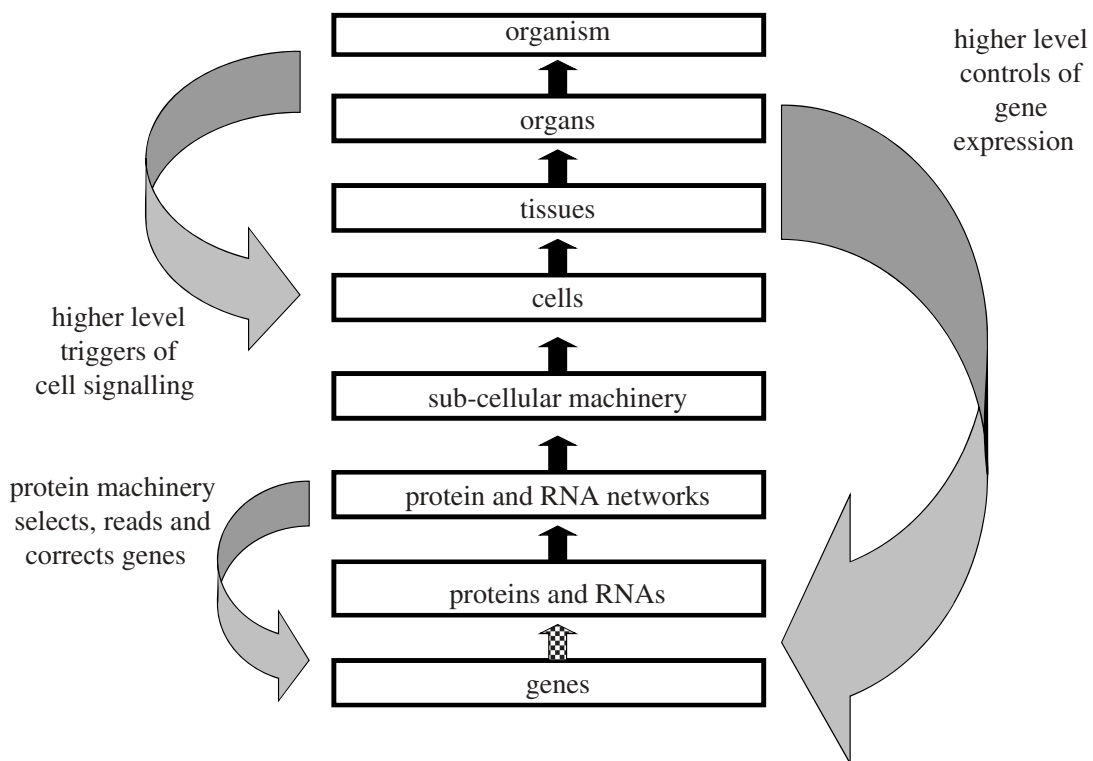


Figure 0.1.: Upward and downward causation in biological systems. Upward pointing arrows represent causalities in the reductionist view. Downward pointing arrows indicate different feedback mechanisms, where entities on emergently higher levels influence processes on the constituting lower levels [Noble (2011)].

Based on insights gained from a mathematical model of the human heart that showed the necessity of downward causation for proper functioning on the lower levels, Noble (2011) proposed a theory of biological relativity to relax the classical reductionism (Fig. 0.1). Today, it is possible to follow this systemic view via multiscale modelling and the integration of experimental data from molecular up to environmental scales [Qu *et al.* (2011)].

Other examples of downward causation in biological systems range from epigenetics to psychosomatic medicine. On occasion of Darwin's 200th birthday, Mattick (2009) discussed the possibility of inheritance of learnt features by RNA-directed epigenetic mechanisms. Benedetti (2008) showed, how placebo effects take effect from the psychosocial level of an individual down to the molecular level.

Mechanical feedback, as proposed by Shraiman (2005), is one possible mechanism by which larger structures such as tissues may control the dynamic behaviour of the constituting smaller elements such as cells. Mechanosensitive protein complexes are capable of translating mechanical into chemical signals and vice versa, thereby governing cellular behaviours like growth, proliferation, and migration [Lecuit (2010), Ingber (2008) and Schwarz (2004)]. They are prime candidates on the molecular level for executing phenomena such as the substrate stiffness-dependent differentiation of mesenchymal stem cells into diverse cell types, as described by Engler *et al.* (2006).

In our work, we use cell density as a read-out for the state of the micromechanical environment and correlate it with cellular parameters such as motility and proliferation. In this respect, we investigate a feedback mechanism from the tissue scale onto the sub-cellular machinery.

1. Introduction

This chapter gives at first a general introduction to epithelial tissues and their significance in physiology and disease of metazoans. The second part introduces our cell line model. Third and fourth part provide an introduction on cellular proliferation and motility, respectively, and describe our current knowledge of these phenomena (i) on the single cell level and (ii) in the tissue context and (iii) considering special cases relevant to the work presented in this thesis. The fifth part summarises a selection of computational models of tissue growth. Finally we summarise what will be shown in this dissertation.

1.1. Epithelial tissues

Evolutionary, epithelia are the the oldest type of cellular tissue. The first simple multicellular organisms consisted of two-dimensional and often folded sheets of epithelial cells [Baum *et al.* (2008)]. About 600 million years ago, gastrulation evolved, a milestone in the history of life. During this process, a group of cells invaginates from the blastula, a hollow sphere of epithelial cells, and detaches from its tissue network. Eventually, gastrulation leads to the separation of the three germ layers that give rise to all cell types of animal tissues: endoderm, mesoderm and ectoderm. From these three layers a much greater variety of tissue and organ types could evolve, giving rise to the complexity found in metazoan organisms. Today we classify the tissues that constitute metazoans into four types: Epithelial, muscle, nervous and connective tissue, each one highly specialised in morphology and function [Thiery & Sleeman (2006) and Shook & Keller (2003)].

In modern metazoans, epithelial tissues cover the surfaces of organs and cavities. Thus, their proper functioning is responsible for the regulated transport of nutrients, signaling molecules, and waste, as well as for the protection of the organism and its organs. Fig. 1.1 shows different kinds of epithelia and their functions in the human body.

In the kidney, simple cuboidal epithelial cells, which we use for our experiments (sec. 1.2), line the tubules, which constitute the nephrons, which in turn are the functional units of a kidney. These epithelial cells are responsible for the regulation of the ion content in the blood, the absorption of sugar from the blood, and water retention from the urine [Marieb & Mitchell (2009)].

An epithelium can have quite diverse morphologies, ranging from monolayered or multilayered two-dimensional sheets to branched tubular networks. In the fully differentiated state, different types of cell-cell junctions are a common feature of epithelial tissues, resulting in a strong cohesion of the tissue and the two-dimensional functionality based on its apicobasal polarity. Furthermore, epithelia can exhibit planar cell polarity (PCP), i.e. an orientation of structures within the tissue plane [Wang *et al.* (2012), Nelson & Bissell (2006) and Hagios *et al.* (1998)].

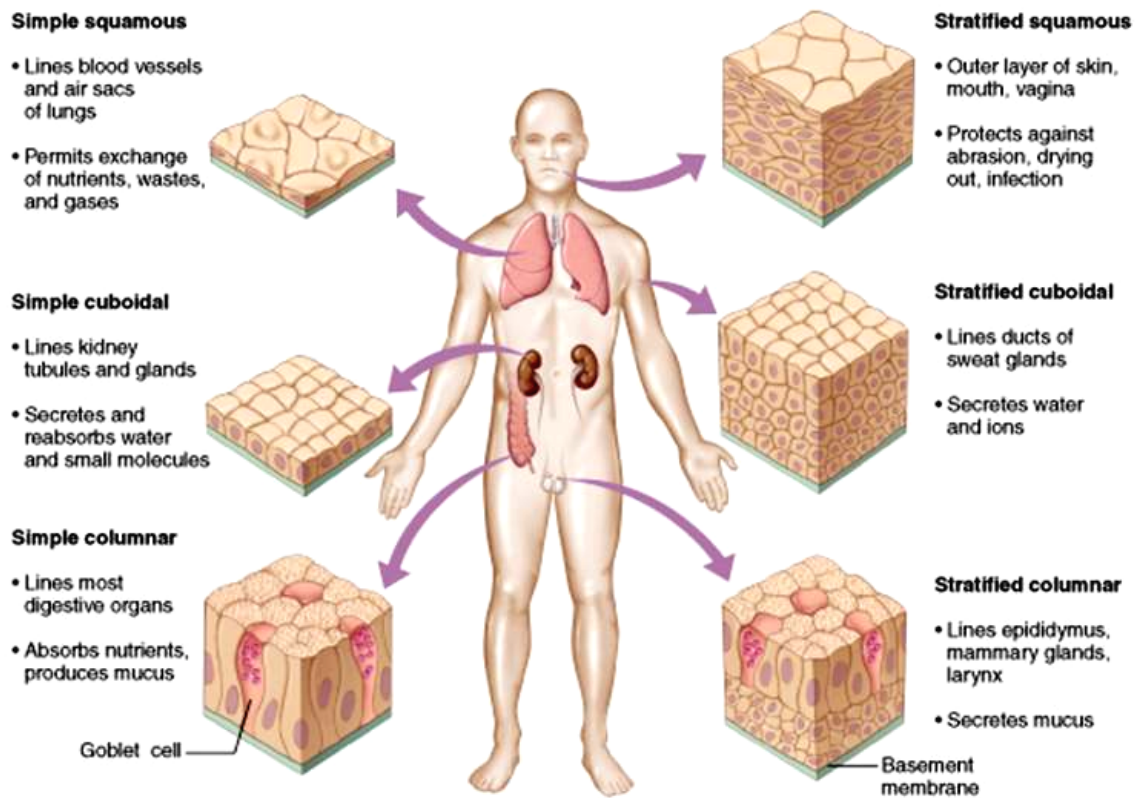


Figure 1.1.: Epithelial tissues and their functions, covering surfaces of organs and cavities in the human body. The common feature of epithelia is their 2-dimensional functionality of separating an inside from an outside and regulating transport of nutrients, signaling molecules and waste [Marieb & Mitchell (2009)].

Another reason for the intense studies of epithelia is comes from the notion that more than 90 % of all human cancers are of epithelial origin, as found by three studies in Denmark between 1943 and 1967 [Cairns (1975)].

Processes in which well differentiated epithelial cells adopt a more motile and less connected, mesenchymal-like phenotype are called epithelial-mesenchymal transitions (EMT) and are observed not only during gastrulation but also in disease. They

are thought to play an important role in the progression of metastasising carcinoma, i.e. epithelial cancers [Nisticò *et al.* (2012) and Levayer & Lecuit (2008)]. This idea originates from the 'seed and soil' hypothesis formulated by the surgeon Stephen Paget in 1889. From observations of the frequency of secondary cancers in patients he derived the idea that cancerous cells - the seeds - detach from their normal tissues and migrate through vessels to distant organs, where they settle down and metastasize only in organs favouring their growth - the soil [Fidler (2003)].

However, Christiansen & Rajasekaran (2006) collected several examples of metastasizing cells that only partially underwent an EMT, suggesting that EMT is not a necessary precondition for cancer progression (Fig. 1.2). Moreover, Bergstralh & St Johnston (2012) showed that in *Drosophila* the distorted cell division of an epithelial cell - leading to the extrusion of one daughter cell - is not sufficient for it to leave the compound structure and become malignant, but immediately is fixed.

In more detail the EMT scenario of cancer progression now looks as follows (Fig. 1.2): The expression of matrix metalloproteinases (MMPs) leads to an increased invasiveness of clusters of epithelial-like cells, which enter the surrounding extracellular matrix (ECM). Decreased cohesiveness via the degradation of cell-cell junctions such as E-Cadherin-dependent adherence junctions promotes excessive proliferation and again invasiveness. A further transformation towards the mesenchymal phenotype in some cases completes the EMT. According to Christiansen & Rajasekaran (2006), in all these phases clusters of cells or single cells can become malignant, travel through vessels to distant organs and, if conditions are suitable for them to attach, form secondary tumors and possibly undergo the reverse process, an mesenchymal-epithelial transition (MET).

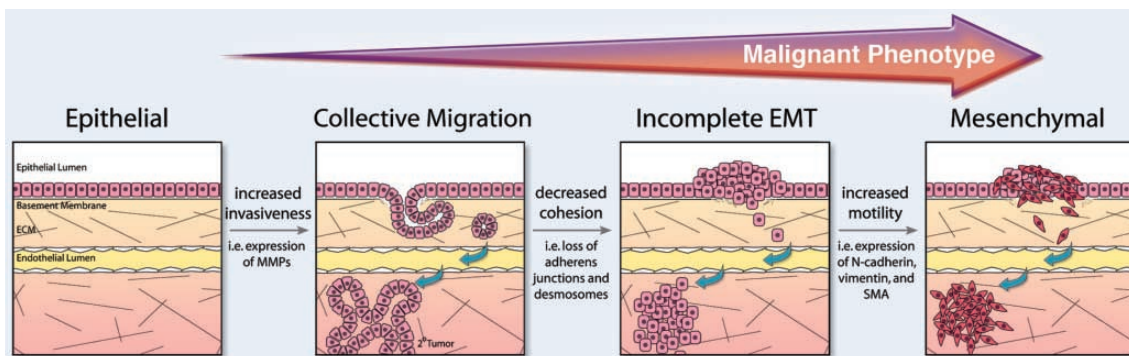


Figure 1.2.: Tumorigenesis, adopted from Christiansen & Rajasekaran (2006). Epithelial cells detach from their tissue as groups or as individual cells, after partial or complete epithelial-mesenchymal transition (EMT) and via transport through vessels reach distant organs, where secondary tumors can form. Eventually cells revert to an epithelial phenotype again (MET).

Each of the steps described above is governed by the interplay of complex signaling networks and physical properties of the system [Tanos & Rodriguez-Boulan (2008)]

and Thiery & Sleeman (2006)].

To study some aspects of EMT and its inverse, MET, *in vitro*, there are two widely used experimental setups.

The scratch-wound assay simulates a wound healing process, in which the wounding is initiated by scratching an epithelial cell layer or by removing a barrier at the edge of a confluent tissue. Subsequently, it can be observed how cells exit contact inhibition of proliferation (sec. 1.3), re-enter the cell cycle and fill the open space [Treat et al. (2009), Garcia-Fernandez et al. (2009), Bindschadler & McGrath (2007) and Poujade et al. (2007)].

A model for MET is the transition of epithelial cells growing from an initially mesenchymal-like phase of low cell density into a polarised epithelium (see next section) [Zegers et al. (2003)].

1.2. Cell line model MDCK-2

Our model system is the Madin-Darby Canine Kidney cell line MDCK-2, which is a widely used model for studying epithelial biology. These cells were initially derived from the kidney of a normal adult female cocker spaniel in September 1958 by S.H. Madin and N.B. Darbin [Gaush *et al.* (1966)] and subsequently subcloned to yield a more homogeneous cell population with epithelial characteristics. MDCK cells are immortal, i.e. they proliferate over infinite generations, if nutrient and growth factor conditions are appropriate. In contrast to some cancer cell lines, they exhibit contact inhibition of proliferation (CIP), which is a form of growth control at high cell densities and will be explained in sec. 1.3.

Seeded on a two-dimensional substrate at low density, i.e. significantly before confluence, MDCK cells show high motility and proliferation rate, i.e. a rather mesenchymal-like behaviour (left image in Fig. 1.3). After several generations of cell divisions and therefore an increase in cell density, their behaviour changes dramatically. The cell collective becomes epithelial in terms of motility, proliferation and polarity, which now distinguishes the basal from the apical side of the cells (right image in Fig. 1.3). The dynamics of this transition will be further described in later sections of this introduction and a contribution is given by our results (see chapter 2).

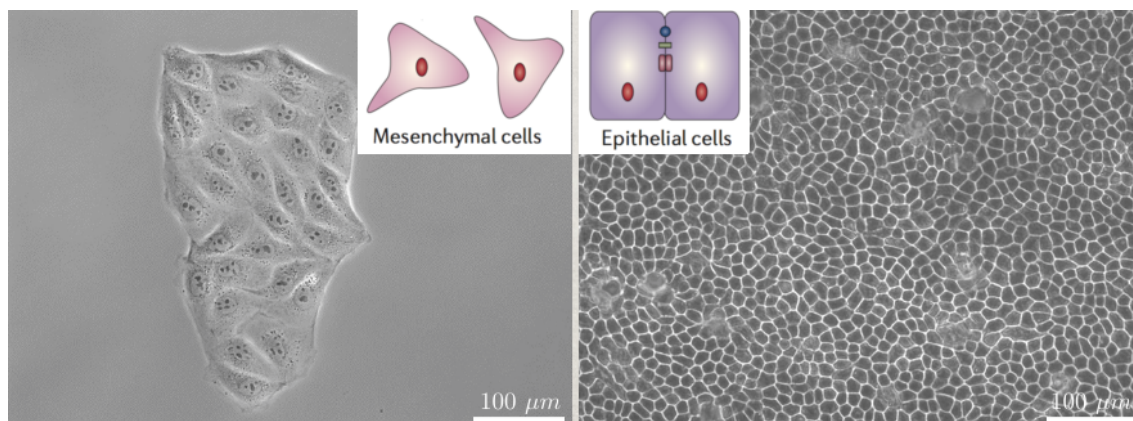


Figure 1.3.: MDCK-2 cells, grown on a glass surface. Within two weeks the cells develop from a very motile state with high proliferation rate and rear-front polarity (left side) into an epithelium, characterised by low motility and proliferation rate and a basal-apical polarity (right side). Insets: Schematic rear-front polarity (left) and basal-apical polarity (right) adopted from Thiery & Sleeman (2006).

Following the development of a colony of MDCK cells into high density, i.e. post confluence, and the associated arrest of proliferation, these cells differentiate into a functional epithelium, that carries out the transport of bulk from the apical to

the basal side. In case cells are grown on an impermeable substrate, this leads to the formation of domes, which are hemicysts lifting themselves above the epithelial plane until they collapse. The resulting hole in the tissue is subsequently repaired by increased proliferation of neighbouring cells. This effect also depends on the strength of adhesion between the cells and the substrate and can be chemically inhibited or promoted [Thomas *et al.* (1982) and Rabito *et al.* (1980)].

Misfeldt *et al.* (1976) characterised the transepithelial transport of water and ions by measuring flux and resulting electrical potential. Tanner *et al.* (1983) described a physical model, concerning geometry and forces of the domes and Hoh & Schoenenberger (1994) measured mechanical properties of MDCK monolayers using atomic force microscopy (AFM).

Elia & Lippincott-Schwartz (2001) describe the culturing of MDCK cells in a three-dimensional environment mimicking the extracellular matrix (ECM). Here the same cells behave very different compared to the two-dimensional setup and form spherical cysts, in which the apical side of a monolayer of polarized cells points towards the hollow lumen [Schwartz & Chen (2013) and Zegers *et al.* (2003)].

For our work we used clones of the MDCK-2 cell line with fluorescently labeled histones growing on a two-dimensional glass surface (chapter 5, materials & methods).

We now look bottom-up into details of cellular mechanisms concerning proliferation and motility in individual cells and in the tissue context.

1.3. Proliferation

In this section we consider basic aspects of the eukaryotic cell cycle, ranging from the molecular level to regulation of proliferation in the tissue and organismal context.

The Cell Cycle

The biological cell is the smallest known unit of biochemical life and is capable of energy and information management and self-reproduction [Cooper & Hausmann (2008)]. Signaling networks integrate various inputs and regulate the transitions between fundamental cellular functions such as cell growth and proliferation, cell survival and death, cellular motility (sec. 1.4), and terminal differentiation, i.e. the change in gene expression patterns leading to the fully specialized and growth-arrested state of a cell, in which it carries out its physiological functions [Lecuit & Goff (2007)].

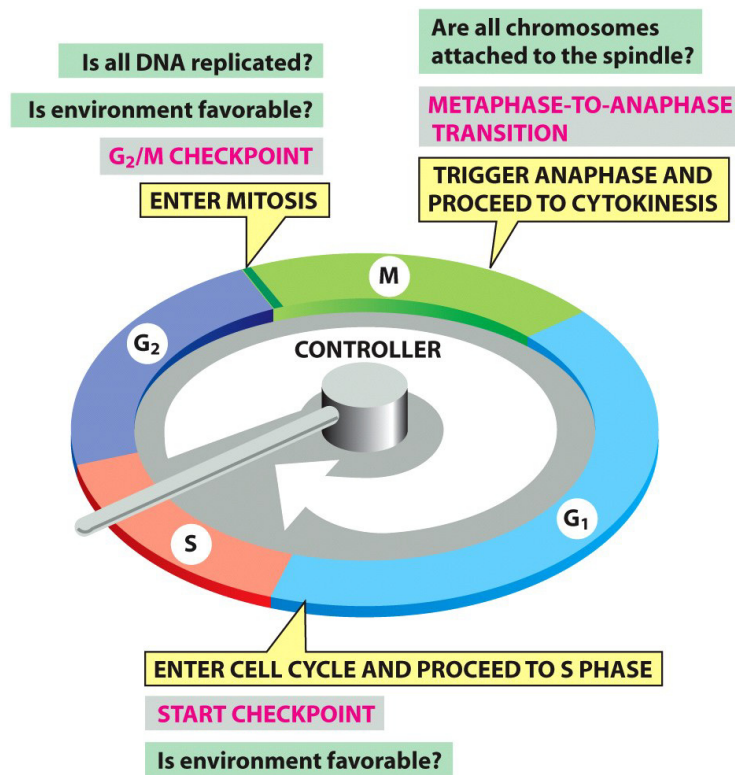


Figure 1.4.: The cell cycle and its checkpoints

Proliferating cells traverse through the phases gap 1 (G₁), DNA synthesis (S), gap 2 (G₂) and mitosis (M), passing by several checkpoints at which internal and external parameters are being monitored. [Alberts *et al.* (2007)]

One of a cell's most obvious features is therefore the cell cycle, which describes the different phases preceding cell division (Fig. 1.4).

The eukaryotic cell cycle is controlled by cyclins, which are proteins that cyclically accumulate and degrade during the cell cycle. They activate cyclin-dependent kinases (CDKs), which in turn activate or inhibit processes required to drive each cell cycle phase. A proliferating cell traverses the cell cycle through the phases G1 (gap 1), S (DNA synthesis), G2 (gap 2) and M (mitosis and cell division). Upon terminal differentiation cells enter the resting phase (G0, not shown in figure); this step is often induced by reduced growth factor signaling and is in some cases reversible [Nurse (2000)].

In metazoans, where cells are embedded in tissues and organs, cell cycle control is extremely important to prevent excessive proliferation. At each checkpoint, internal (e.g. quality of DNA, cell size) and external parameters (e.g. availability of nutrients and growth factors, mechanical properties of the microenvironment) are evaluated before executing the next steps in the cell cycle program (Fig. 1.4) [Alberts *et al.* (2007)].

Contact Inhibition of Proliferation

In particular, the checkpoint before the G1-S-phase transition (Start Checkpoint in Fig. 1.4), which is also called 'restriction point' in animals, is of major importance for tissue homeostasis. In cultured cell collectives the phenomenon that causes cells to exit the cell cycle before they overcome the restriction point is called 'contact inhibition of proliferation' (CIP, Fig. 1.5). Cancer cells are often characterized by a loss of CIP. However, this term is misleading, since it requires more than cell-cell contacts, i.e. the tight association of transmembrane proteins of neighbouring cells, to induce CIP. Instead, additional parameters like cell size, cell shape, and mechanical constraints have an influence on a cell's proliferation behaviour [Puliafito *et al.* (2012)].

The decrease of cellular motility [Abercrombie & Heaysman (1953)] and the growth arrest of non-cancerous cultured fibroblasts following the establishment of cell-cell contacts [Abercrombie & Heaysman (1954)] was first described in the 1950s.

In the 1960s, Castor performed growth experiments and employed the scratch-wound assay to study proliferation control in several epithelial-like cell lines (1S1, 3T3, and 3C4) as well as in cancer cell lines (1S13 and HeLa) [Castor (1968)]. By using time-lapse microscopy, Castor observed a decrease in cellular volumes after the cell collective had reached confluence, i.e. complete coverage of the substrate surface by cells. He also described a high proliferation rate in the leading edge of the wounded tissue while it was invading free space.

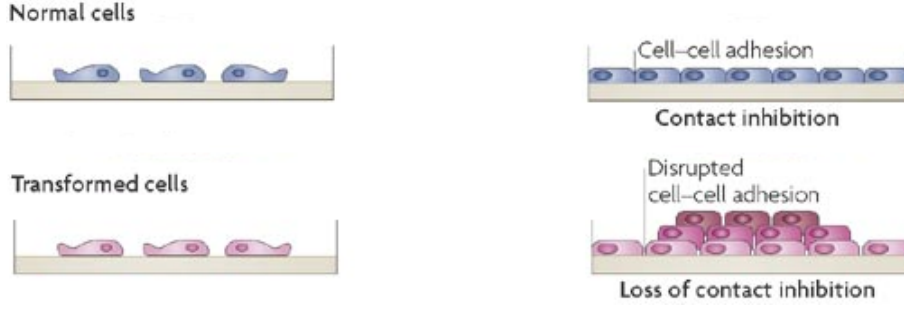


Figure 1.5.: Contact inhibition of proliferation following confluence in non-cancerous cell culture (top, cf. Fig. 1.3); in contrast, many cancerous cells (bottom) proliferate excessively leading to a piling up of cells. [Takai *et al.* (2008)]

Castor suggested that CIP is simply regulated by the cells' changing surface and therefore by their ability to uptake growth stimulating substances. He found a characteristic mitotic density curve, which showed that the proliferation rate of non-cancerous cells starts decreasing immediately after reaching confluence. Interestingly cellular motility decreased already at lower cell densities. In contrast, cancerous cell lines do not exhibit a decrease in motility and proliferation rate drops only at much higher cell densities [Castor (1972)].

In a recent study, our group and collaborators showed a strong correlation between cell areas, A , and cell division times, $T(A)$, within the confluent regime of growing colonies of MDCK-2 cells (sec. 1.2). Cell area-dependent division times were calculated using a model that is based on the temporal change of cell area distributions, $P(A,t)$, due to cell divisions:

$$\frac{\partial P(A,t)}{\partial t} = 2 \cdot \frac{P(2A,t)}{T(2A)} - \frac{P(A,t)}{T(A)} \quad (1.1)$$

The two terms on the right hand side describe the change in number of cells having the area A . The first term represents cells having the area $2A$ and dividing with a rate of $1/T(2A)$ into 2 cells of area A , and the second term represents cells having the area A and dividing with a rate of $1/T(A)$ into 2 cells of area of $A/2$. Fig. 1.6 shows the evolution of area distributions over time and the derived division times [Puliafito *et al.* (2012)].

CIP also plays a role *in vivo*, especially in embryonic development, organ size control, and tissue regeneration, and loss of CIP is a hallmark of cancer (sec. 1.1). In mammals, E-cadherin, a transmembrane protein involved in cell-cell contacts, activates the Hippo pathway, a signalling pathway that inhibits proliferation. A

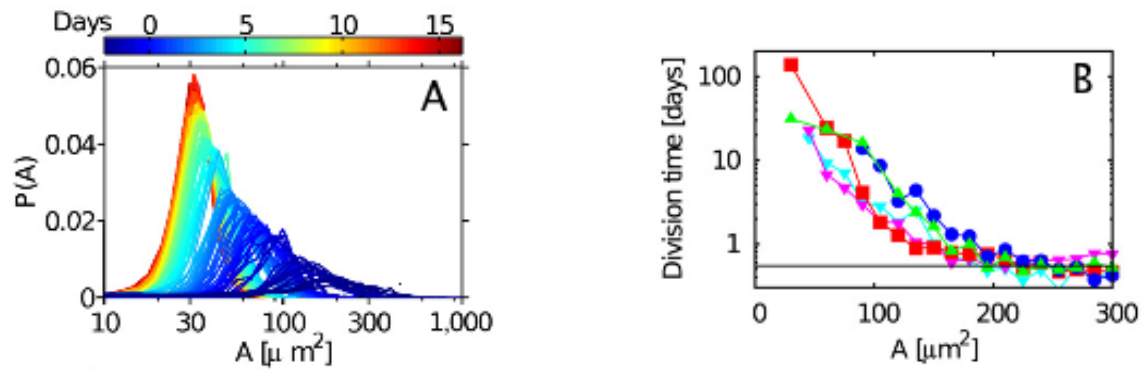


Figure 1.6.: Cell area-dependence of division times in cultured MDCK-2 cells [Puliato *et al.* (2012)]. A: Post-confluent cell area distributions $P(A)$ over 2 weeks. B) Division times $T(A)$, derived from data in A using Eq.1.1, show a strong increase for cell areas $A < 200\mu\text{m}^2$

homolog pathway is known in *Drosophila* [Zhao *et al.* (2011)]. Using micropatterned substrates of well defined sizes Wada *et al.* (2011) showed that cell shape is another important factor in the regulation of the Hippo pathway and proposed the model shown in Fig. 1.7.

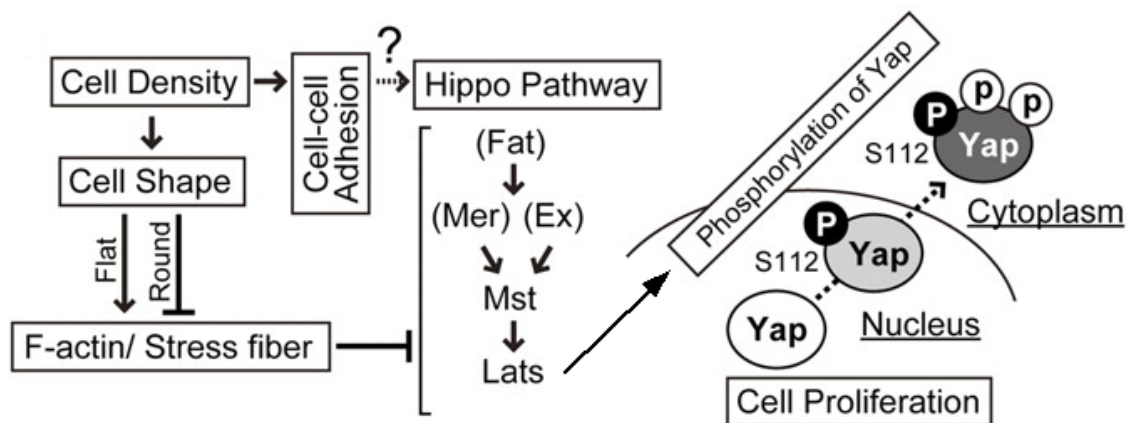


Figure 1.7.: Model of density- and cell shape-dependent regulation of the Hippo pathway and downstream phosphorylation of Yap, eventually leading to an arrest of cell proliferation. Modified from Wada *et al.* (2011).

At higher cell densities cell-cell adhesions strengthens and cells undergo a transition from a flat morphology with more stress fibers to a round morphology with less stress fibers. Cell adhesions promote the phosphorylation of Yap via a signaling cascade involving Fat, Merlin (Mer), Expanded (Ex), Mst/Hippo, and Lat. Lats in turn phosphorylates the major downstream effector Yes-associated protein (YAP). Upon phosphorylation, nuclear YAP relocates to the cytoplasm, where it is unable

to promote cell proliferation and thereby leads to cell cycle arrest [Kim *et al.* (2011) and Morrison *et al.* (2001)].

In addition Wada *et al.* (2011) showed that the increased presence of stress fibers inhibits the Hippo pathway upstream of or at the level of Lats, which is consistent with other findings that not cell-cell contacts alone trigger CIP, but increased cell density leading to the rounding of cells is another required condition.

Basan *et al.* (2010) designed a reaction-diffusion model for the system comprising E-cadherin, α - and β -catenin to describe CIP. The model is based on the assumption that there is a competition between α -catenin- β -catenin complexes (in case of motile cells with branching actin networks) and α -dimers (in case of confluent cells with β -catenin-E-cadherin complexes in cell-cell contacts).

A process akin to CIP seems to be present in fission yeast, where in response to hydrostatic pressure the G2 cell cycle phase is delayed, and this effect is independent of cell size, cytokinesis and DNA damage [George *et al.* (2007)].

Proliferation Patterns

In this section we review how cell divisions happen to cluster in space and time during tissue growth.

Koch (1980) analysed the nature of cell cycle variations in mouse cell lines and in the bacterium *Staphylococcus albus* to show that they cannot be explained by a combination of a constant cycle duration and the influence of a single chance event with constant probability. Investigating cell cycle distributions in budding yeast, Talia *et al.* (2007) proved that one contribution to cell cycle variability originates from molecular noise in gene expression that is responsible for driving the cell cycle. In addition they assume a size-sensing module to allow for a compensation of variable growth rates.

Based on their study in Chinese hamster ovary cells, Darzynkiewicz *et al.* (1982) suggest a mechanism of cell cycle desynchronisation due to asymmetric cell division in the sense that metabolic cytoplasmic constituents are not distributed equally among the daughter cells and hypothesize that an equalisation point arrests cells in the cell cycle until a critical RNA content is attained.

Milán *et al.* (1996) studied proliferation patterns in the imaginal wing primordium of *Drosophila melanogaster* and found that clusters of neighbouring cells were in the same cell cycle phase. Similarly, Cai *et al.* (1997) measured the cell cycle variability in different regions of the embryonic mouse cortex and found that it is less than 10%.

A promising approach was used in the study by Chiorino *et al.* (2001). Starting with cultured human cancer cells that exhibited synchronous cell cycle progressions

they analysed the progress of their desynchronisation by assessing the mean and standard deviation of their cell cycle durations [see also Khaladi & Arino (2000) and Arino & Sánchez (1997)].

We assume that, under conditions that promote maximal cell proliferation, cells generally traverse the cell cycle more or less regularly. Whenever the distribution of cell cycle periods for a specific cell type has a finite width, which is smaller than its mean, clustering of dividing cells would occur locally in space and time, as found in the studies mentioned above. In chapter 2 we present our study using the non-cancerous cell line MDCK-2 to further investigate the causes of these cell cycle correlations and the mechanisms leading to their desynchronisation.

Division axis orientation

In the previous sections we concentrated on the question as of how growth is regulated during epithelial tissue morphogenesis and how cells decide whether and when to divide. In order to adopt their correct architecture, developing tissues also have to ensure that cells end up at the correct position within the tissue. Therefore, another factor of great impact is the orientation of division axes (Fig. 1.8) [Lecuit & Goff (2007)].

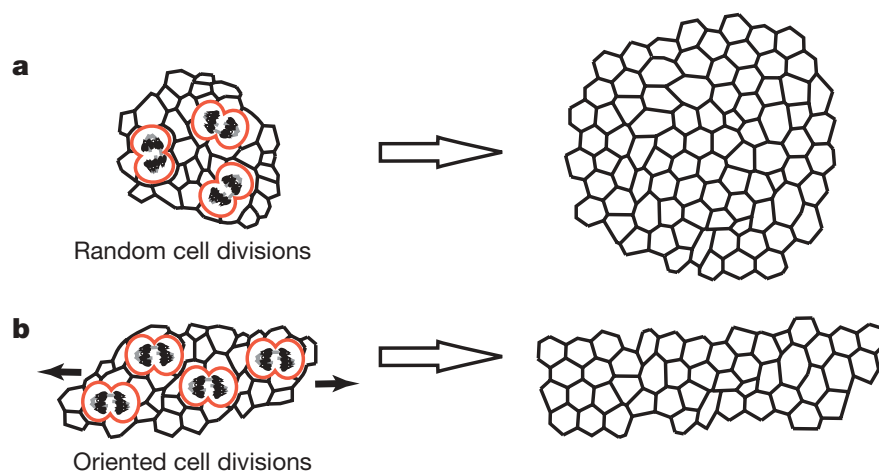


Figure 1.8.: Random (a) versus oriented (b) cell divisions and their impact on tissue shape, modified from Lecuit & Goff (2007).

Concha & Adams (1998) showed that in the gastrula and neurula stages of zebrafish development expansion of the tissue is achieved by a systematic orientation of cell divisions along the anterior-posterior body axis. This can be explained by

the activity of planar cell polarity pathways [Jones & Chen (2007) and Gong *et al.* (2004)].

Other work suggests that in many cases it is solely the mechanical microenvironment, reflected in a cell's shape, that determines the orientation of the cell division axis (see Gibson *et al.* (2011) and Strauss *et al.* (2006) for experimental and Alim *et al.* (2012) and Li *et al.* (2012) for theoretical contributions).

In plant cells the division plane is determined by the interplay of the cytoskeleton and cell shape. In the absence of other cues, a cell plate of minimal area generates two daughter cells of similar size (Errera's rule), Besson & Dumais (2011).

In our second study (chapter 3), we find a correlation between the direction of a cell's migration and the division axis, but also completely uncorrelated mother and daughter migrations.

1.4. Motility

Besides cell proliferation, motility is another basic feature of living cells. Obviously, the ability to move in order to find food or escape threats is a crucial evolutionary advantage for all organisms. Some organisms such as social amoebae use chemotaxis-directed migration to aggregate and temporally form a multicellular organism in case of starvation to increase the chance of a colony's survival. Likewise, collective cell migration represents an important feature in many biological functions in multicellular organisms, such as embryonic morphogenesis and tissue repair, and in dysfunctions like cancer invasion.

Single cell migration

"Polarity is intrinsic to a migrating cell [Ridley *et al.* (2003)]", since form and function in cell biology are hardly separable and migration needs a direction. Herant & Dembo (2010) demonstrated how cell polarity, i.e. spatial differences in form and function within one cell, leads to the ability of performing different directed migration modes.

Fig. 1.9 shows central elements of the treadmilling machinery that is used for cellular migration on. The small GTPases Rho and Rac (besides Cdc42 and Ras) constitute a bistable reaction-diffusion system that polarises the cell. Rac in the front of the migrating cell promotes actin branching via the Arp2/3 complex and therefore the formation of lamellipodial protrusions and of integrin-mediated focal adhesions (not shown). Rho, which inhibits Rac, leads to a local increase of actin-myosin contraction and the disassembly of adhesions in the rear. The microtubule system supports this machinery by polarised transport of regulatory proteins [Mogilner & Keren (2009), Ridley (2001) and Nobes & Hall (1999)].

It has to be mentioned though, that motile cells in three-dimensional and in effective one-dimensional environments partially use different mechanisms than the one described above [Balzer *et al.* (2012), Wirtz *et al.* (2011), Ridley (2011) and Yamazaki *et al.* (2009)].

An interesting borderline case between single cell and multicellular life is the social amoeba *Dictyostelium discoideum*. *Dictyostelium* normally lives as a unicellular organism performing single cell migration, but under nutrient starvation it undergoes a transformation. Via oscillatory secretion of cAMP (cyclic adenosine monophosphate), up to a million cells organize into aggregates and differentiate. This leads to the development of a motile slug structure and eventually to the differentiation of a fruiting body, which facilitates its own spreading and therefore increases the likelihood of the colony's survival [Weijer (2009) and Palsson & Othmer (2000)].

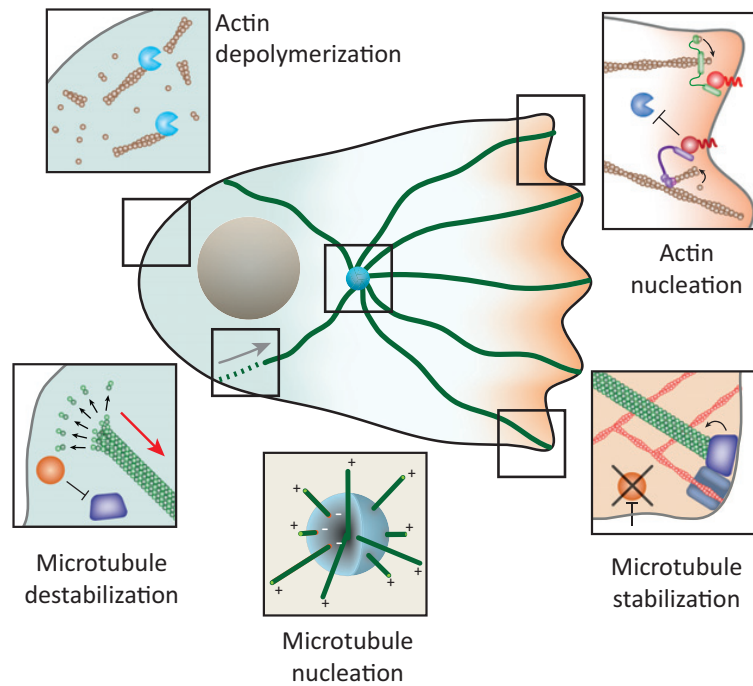


Figure 1.9.: Polarised organisation of the mechanical elements in a cell migrating to the right. In the front of the cell membrane-associated small GTPases Cdc42 and Rac (red) activate actin nucleators such as formin (green) and Arp2/3 (purple) and inhibit actin destabilising factors (blue). Similarly microtubule plus ends are capped and stabilised by EB1 and APC (blue) in the front of the cell. In contrast, in the rear of the cell, the small GTPase Rho, which mutually inhibits Rac, promotes actin and microtubule depolymerisation [Goehring & Grill (2013)].

Collective migration

Cells that are stably connected to each other by adherens junctions have the ability to migrate in a collectively ordered manner. This is typical for groups of epithelial cells.

Three properties are characteristic for collective migration: (i) There is physical and functional connection between the cells throughout their movement. (ii) The actin cytoskeleton has a supracellular structure enabling force transmission and the multicellular system shows polarity. (iii) Especially in developmental processes of collective migration, structural modification of the collective happens as migration progresses [Friedl & Gilmour (2009)].

Kabla (2012) simulated a variety of collective migration modes based on a model of cells with two intrinsic parameters, motility and mechanical cell-cell adhesion. Also Borghi *et al.* (2010) investigated how the cellular motility behaviour is influenced by expression ratios of cell-substrate and cell-cell adhesion molecules, i.e. integrin- and cadherin-mediated adhesions. Similarly, Montell (2008) assumes four basic mechan-

ical properties to allow for a diversity of morphogenetic cell movements: cell-cell adhesion, cell-substrate/matrix adhesion, the ability to form protrusions, and contractility.

Theveneau *et al.* proposed a model that describes how mesenchymal cells can undergo collective migration. It assumes that the mutual inhibition of the small GTPases Rho and Rac (see previous section on single cell migration) not only occurs within one cell, but expands to neighbouring cells, and thereby leads to an alternation of repulsion and attraction [Theveneau & Mayor (2011), Theveneau & Mayor (2010) and Mayor & Carmona-Fontaine (2010)].

Cultured MDCK cells also exhibit collective migration. Petitjean *et al.* (2010) measured velocity fields of MDCK cells grown on PDMS (Polydimethylsiloxane) membrane. Consistent with our own work (chapter 3), they demonstrate a decrease of cellular velocities with increasing cell density.

Angelini *et al.* (2011) describe the dynamics in a confluent monolayer of MDCK cells as glass-like, and find an increase in the heterogeneity of velocities as cell density increases.

Trepat & Fredberg (2011) developed the concept of plithotaxis, i.e. "the tendency for each individual cell within a monolayer to migrate along the local orientation of the maximal normal stress, or equivalently, minimal shear stress."

Rotating cell collectives

Now we look into special cases, *in vivo* and *in vitro*, where groups of cells migrate collectively in a manner resulting in rotations of the whole colony (Fig. 1.10).

Haigo & Bilder (2011) showed that polarised rotation of the follicle epithelia in the developing *Drosophila* egg is required to polarise the fibrillar extracellular matrix (ECM), which in turn constrains the shape of the growing tissue, and leads to its elongation (Fig. 1.10 A).

Another example of morphogenetic rotations of groups of cells are the photoreceptor progenitors in the developing *Drosophila* eye [Escudero *et al.* (2007)].

Similarly, human breast cell lines cultured in a three-dimensional matrix exhibit collective angular motion (Tanner *et al.* (2012)). Single cells performed multiple rotations, maintained the sense of rotation after cell divisions, and the collective rotation generated polarised acini (Fig. 1.10 B). However, malignant counterparts of these cell lines did neither perform the collective rotation nor generate acini, indicating that these human epithelial cells actually performed a developmentally relevant function by rotating in an organised manner.

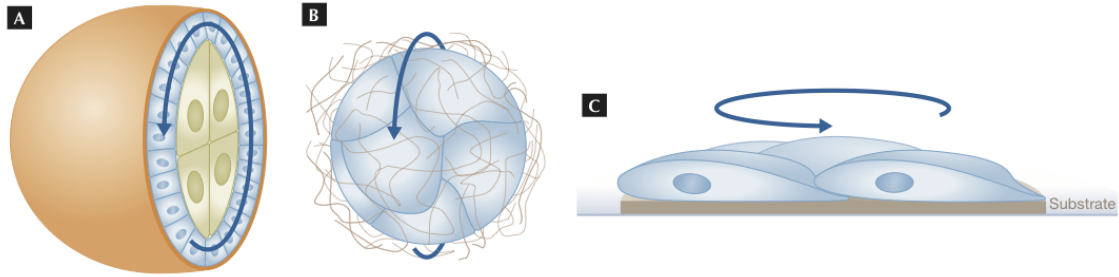


Figure 1.10.: Epithelial rotation. A: Rotating follicular epithelium (blue) along the ECM-basement membrane (orange) leading to an elongation of the *Drosophila* egg. B: Human breast cell line cultured in 3D gel matrix rotating coherently in one direction. C: Symmetry breaking in a group of cells migrating on a micropatterned substrate. Adapted from Rørth (2012).

The symmetry-breaking in mammalian collective cell migration described by Huang *et al.* (2005) resembles the one described above in two dimensions. They plated BCE cells on micropatterned substrates to observe the rotationary migration behaviour and came to the conclusion that there must be an internal symmetry-breaking event involved (Fig. 1.10 C), for which they postulate three conditions. One of these is a physical constriction of space on the micrometer scale, which we can disprove using our spatially unconstrained setup.

We have analysed MDCK-2 cells performing collective rotations on a glass surface without any barriers on the micrometer scale and demonstrate a specific pattern in changes of the sense of these rotation (chapter 3).

1.5. Computational models

Mathematical modelling can provide descriptions of biological systems that coherently unify processes over different temporal and spatial scales and produce testable predictions [Qu *et al.* (2011) and Engler *et al.* (2009)]. We now look into a few examples of modeling approaches to better understand the growth dynamics of epithelial tissues.

Gibson *et al.* (2006) described the emergence of order in epithelia in terms of the distribution of different polygons displayed by cell shapes. Therefore they used a discrete Markov model, which quantifies the changes in cell-cell interfaces during mitoses. Their finding was that the distribution of cell shapes converges to the same distribution independent of the chosen initial distribution and is experimentally well confirmed for different species.

In the *Drosophila* wing development cell competition, i.e. the appearance of unequal division rates in different clusters of cells, does not lead to distortions, but is compensated by an adaptation of proliferation and apoptosis rates [Edgar & Lehner (1996)]. Following this observation, Shraiman (2005) suggested mechanical feedback as a possible regulator for growth control (see Fig. 1.11).

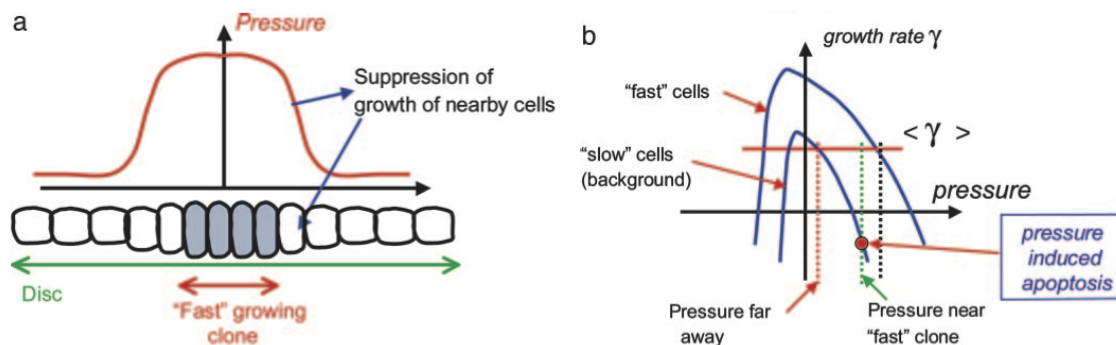


Figure 1.11.: Mechanical feedback as a growth regulator, from Shraiman (2005). a: Accelerated growth within an isolated clone causes compression of nearby tissue. b: The blue curves represent the assumed local and pressure-dependent growth rates γ for fast growing mutant clone cells (upper blue curve) and the slower-growing background tissue (lower blue curve). Negative γ indicates apoptosis, negative pressure means tension. Red line represents the average growth rate of the background. The mutant clone overgrows until the resulting compression (black dashed line) brings its growth rate down to that of the background. Level of compression of wildtype tissue neighboring the clone (green dashed line) may be sufficiently high to trigger the apoptosis of the slower-growing wildtype cells near the clone.

Today, there are several models of tissue morphogenesis comprising a mechanical feedback component. Hufnagel *et al.* (2007) developed a model combining a gradient of the morphogen decapentaplegic (Dpp) and mechanical feedback as an additional regulator for growth control in the *Drosophila* wing disc [Aegerter-Wilmsen *et al.* (2007), Crickmore & Mann (2008)].

Puliafito *et al.* (2012) constructed a model of self-limited epithelial tissue growth, using a one-dimensional vertex model (Fig. 1.12 A). In this model, cell number i is described by two vertices r_i and r_{i+1} and has a preferred length of $L_i(t)$, which is allowed to grow in time, if tension is applied by neighbouring cells. In addition, cells interact with an attachment point R_i on the substrate, which has a friction σ and experiences a random Langevin driving force $\eta_i(t)$. The interactions that occur between vertices and between vertices and attachment points are assumed to be elastic, following Hook's law (eq.1.2). k and κ are parameters, that define the strength of the elastic couplings.

$$H(r_1, \dots, r_{N+1}) = k \sum_{i=1}^N (r_{i+1} - r_i - L_i(t))^2 + \kappa \sum_{i=1}^N (R_i - (r_{i+1} + r_i)/2)^2 \quad (1.2)$$

The dynamics of the attachment points are driven by relaxation of the elastic stress plus random forces representing cellular motility (eq.1.3):

$$\sigma \frac{d}{dt} R_i = - \frac{\partial H}{\partial R_i} + \eta_i(t) \quad (1.3)$$

Fig. 1.12 B, C and D show the simulation results, which closely resemble experimental data for cultured MDCK cell colonies (cf. Fig. 1.6).

Several models were designed to describe more specific properties of growing tissues. They use a continuum mechanics approach with $\rho = \rho(\vec{r}, t)$ representing the local cell density, $\vec{v} = \vec{v}(\vec{r}, t)$ the local velocity and k_d and k_a corresponding to cell source (division) and sink (apoptosis), respectively:

$$\frac{\partial}{\partial t} \rho + \nabla \cdot (\rho \vec{v}) = (k_d - k_a) \rho \quad (1.4)$$

Ranft *et al.* (2010) demonstrated how the introduction of cell division and apoptosis into the continuum mechanical description of an otherwise elastic tissue allows for transitions into a more liquid-like viscous state.

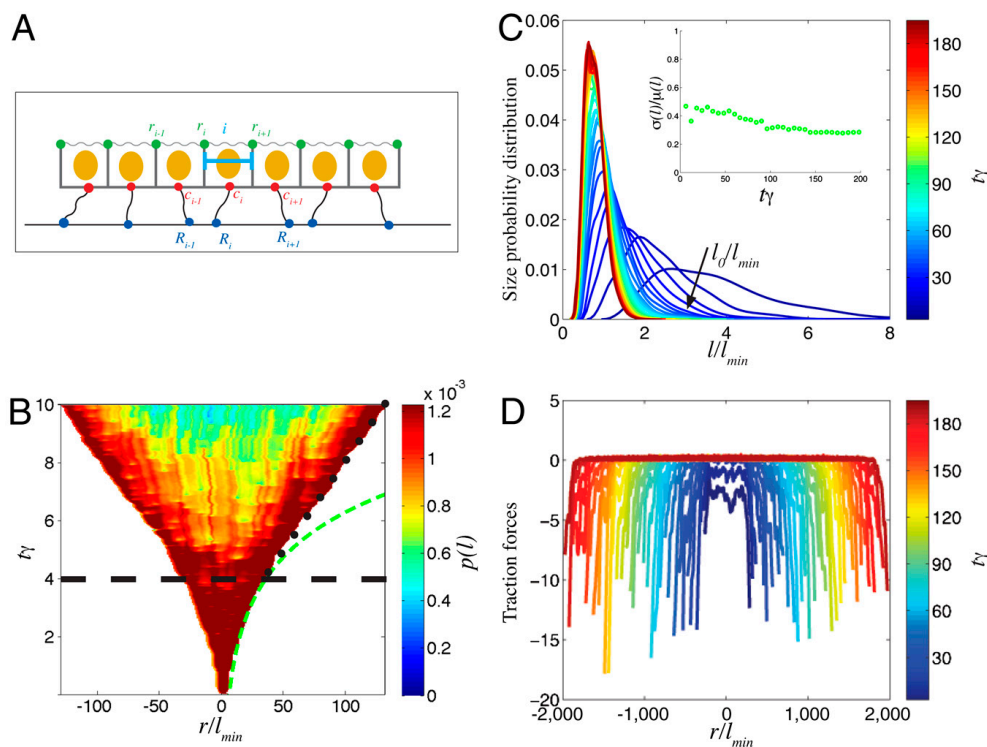


Figure 1.12.: Self-limiting growth model of a one-dimensional adherent cell monolayer [Puliafito *et al.* (2012)]. A: Sketch of the model. Cell i is represented by its two, elastically coupled, vertices, r_i and r_{i+1} . Via another spring the cell is connected to the attachment point R_i . See eq. 1.2 and 1.3. B: Spatio-temporal profile of the proliferation rate. Maximal rate is colour-coded in red. Exponential growth is indicated by the green line. C: The cell size distribution becomes stationary in time (colour-coded). Inset shows coefficient of variation. D: Traction force distribution throughout the colony at different times (colour-coded).

Basan *et al.* (2009) used this approach to follow Stephen Paget’s seed and soil theory of cancer [Fidler (2003)] and investigated the influence of homeostatic pressure on cancer metastases. Basan *et al.* argue that their mechanism of homeostatic competition between different tissues could explain the strong tissue specificity of metastatic growth.

Byrne & Drasdo (2009) compared such a continuum mechanical model with a model based on individual cells for dense monolayers of cultured cells. They assumed a pressure-dependent growth rate and came to similar results like the vertex model of Puliafito *et al.* (2012) regarding global growth dynamics.

1.6. Thesis

This thesis covers two studies on cell cycle correlations (CCC) in epithelial tissue morphogenesis. The first project addresses the origin of these correlations and the dynamics of cell cycle desynchronisation, i.e. the disappearance of these correlations (chapter 2).

Cells in a tissue that arise from a common progenitor cell initially divide synchronously. We investigate this phenomenon *in vitro* and *in silico*. To this end, we use clones of the MDCK-2 cell line expressing a fluorescent nuclear marker to enable automated image analysis and single cell tracking of fluorescence time-lapse microscopy data.

We find that cells go through a decorrelation process, which is an overlay of two independent phenomena: First, a trivial progressive desynchronisation with each generation of cell divisions is due to the stochastic nature of cell cycle periods, which are described by a Gaussian distribution of finite width. Second, an additional non-trivial desynchronisation that occurs above a critical cell density is due to contact inhibition of proliferation, which results in a broadening of the cell cycle distribution and therefore in an acceleration of the desynchronisation process.

We model the progressive desynchronisation of cell cycles mathematically to verify our understanding of the system for the regime of free proliferation. A critical number of generations, after which cell divisions occur regularly distributed in time, was predicted by our model and confirmed experimentally.

In the other project, we investigate consequences of cell cycle correlations for tissue morphodynamics (chapter 3). At low cell density, where we find that MDCK have high motility and maximal proliferation rate, we analyse the patterns of emerging collective migration and investigate how their changes coincide with mitosis.

2. Mitosis patterns in epithelial tissue growth

In this project we characterised cell cycles in growing cell colonies. We quantify the dynamic changes of their probability distributions, their temporal correlations, and their emerging desynchronisation. We then develop a mathematical model to account for the regime of free proliferation at low cell density and propose a possible mechanism for desynchronisation.

2.1. Colony growth

In order to facilitate automated quantification of the properties of growing cell colonies, we first generate fluorescent time-lapse movies of MDCK-2 cells expressing a fluorescently labelled histone marker (H2B-mCherry). We then automatically

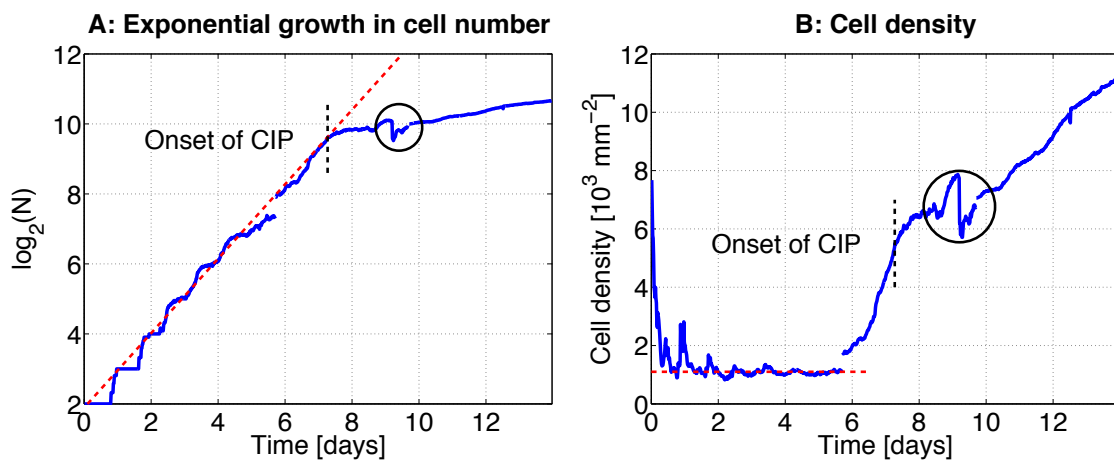


Figure 2.1.: Growing numbers in the developing epithelial cell culture model. A: The number of cells grows exponentially (red line) until the onset of CIP (black line). During the first few generations the stepwise increase displays synchronicity of cell cycles. B: Cell density (calculated by the inverse of mean voronoi cell area, see chapter 5) stays basically constant (red line) for some days until it increases, followed by the onset of CIP (black line). A and B: The emergence of domes is visible in an additional increase of cell number and density, followed by a sudden drop and recovery (black circle). Time=0 represents the start of image acquisition.

segment these images by identifying cell nuclei (chapter 5). From this data, we calculate parameters such as cell number and cell density (Fig. 2.1).

We start image acquisition two generations after seeding single cells, i.e. $\log_2(N) = 2$. The young colony originating from a single parental cell grows essentially exponentially for about one week (Fig. 2.1 A, dashed red line). During the first few days the cell number shows a stepwise increase that reflects the synchronicity of cell divisions for several generations in the young colony. This synchronicity in cell cycles then progressively gets lost (see below). After one week, the increase in cell number drops due to contact inhibition of proliferation (CIP, see black dashed line indicating the transition). At day 9 the sudden changes of cell number are caused by the emergence and disappearance of domes, since cells within the dome leave the focal plane and are therefore not detected anymore.

The average cell density within these colonies is essentially constant for the first 6 days after start of image acquisition (Fig. 2.1 B). This reflects the fact that the expansion of the colony can fully compensate the spatial needs of the newborn daughter cells. The fluctuations in cellular area during this phase originate from the synchronicity of growth.

From day 6 to day 7 cell density increases dramatically. At the same time, the proliferation rate drops, which results in a lesser increase in cell density and ultimately CIP is established. Fluctuations in cell density at day 9 are again caused by the formation and collapse of domes. Afterwards cell number and density increase further with a reduced rate compared to the free proliferation before the onset of CIP.

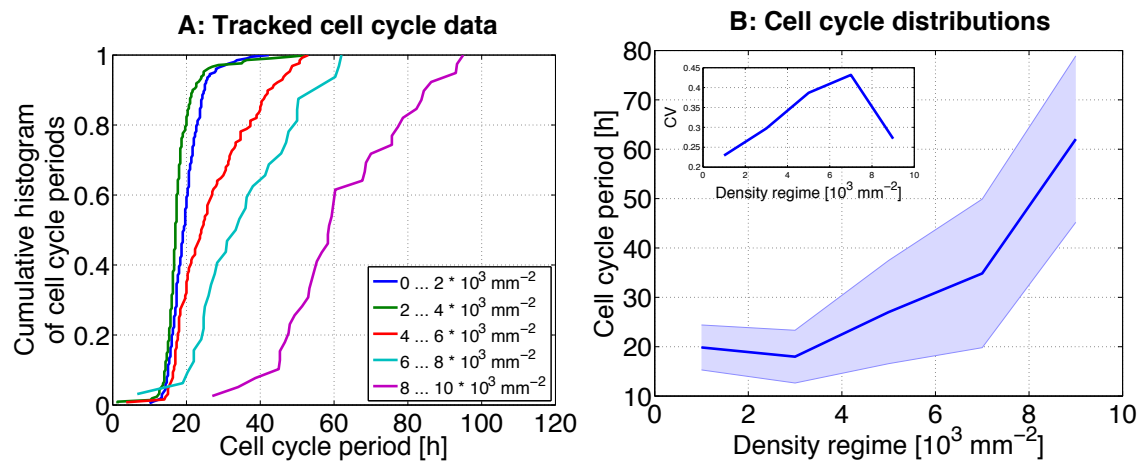


Figure 2.2.: Cell cycle data obtained from single cell tracking and binned into 5 density regimes. A: Cumulative histograms of the data, density regimes are colour-coded, B: Mean (line) and standard deviation (band) of the distributions, binned as defined in A. Inset: Coefficient of variation.

After tracking the individual cells from birth to division and thus obtaining their cell cycle durations (Fig. 5.3), we bin them into five density regimes in order to provide a good categorisation for the different proliferation behaviours. Fig. 2.2 A shows the cumulative histograms of cell cycle periods for the different density regimes (around 1, 3, 5, 7 and 9 $\frac{10^3}{mm^2}$).

In Fig. 2.2 B mean values and standard deviations of the data in A are shown and in the inset the coefficient of variation (CV=standard deviation / mean).

In the lowest two density regimes, from 1 to 3 $\frac{10^3}{mm^2}$, the cell cycle period distributions (CCD) are very similar with the lowest density regime showing a slightly higher mean of the CCD.

The cell cycles in the next two density regimes, around 5 to 7 $\frac{10^3}{mm^2}$, show the strongest variation, most likely because here the cellular density has its fastest increase and the strongest inhomogeneity in cell density emerges (cf. sec. A.2).

In the last regime, around 9 $\frac{10^3}{mm^2}$, the CV decreases again due to the large mean cycle duration (Fig. 2.1 B inset). Longer cell cycle periods are not displayed because of the experimental cut-off.

2.2. Cell cycle correlations

Now we capture the synchronicity of cell divisions via the analysis of age distributions and derive the variability of mean age and spatio-temporal mitosis density (see Fig. 2.3).

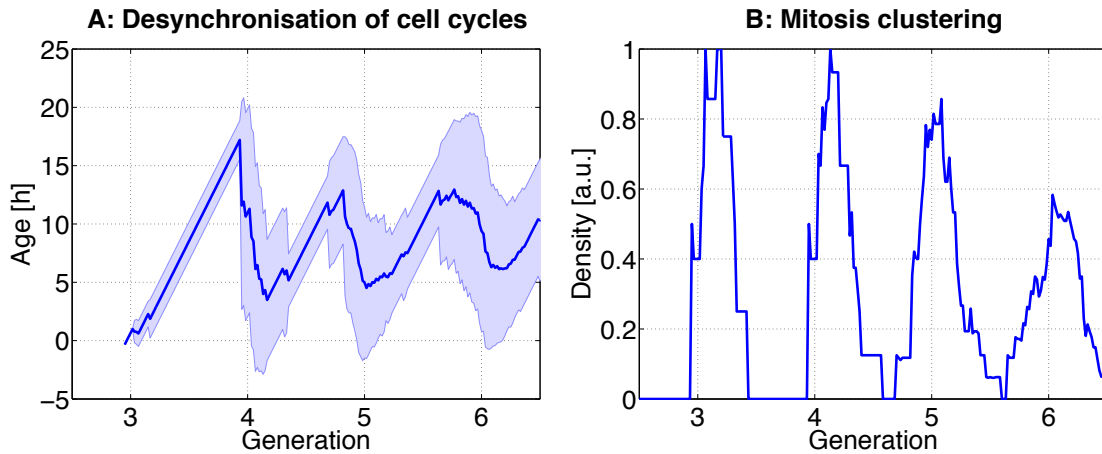


Figure 2.3.: Experimental data. Time in units of standard generation length T_0 (see below). A: Mean (line) and standard deviation (band) of cell age distributions over several generations in the low density regime ($\rho \approx 10^3 \text{ mm}^{-2}$). The distribution gets broader as the cells desynchronise increasingly. B: Decrease of the spatiotemporal mitosis density, defined as the fraction of cells dividing per time. (cf. Fig. 2.5 for simulated data)

We observe an oscillation of the mean age and an increase in the standard deviation of the age distribution, as cells move through the cell cycle collectively before slowly desynchronising (Fig. 2.3 A). Generations are separated in time for six cell divisions (cf. zero values in Fig. 2.3 B).

The temporal clusters of mitosis correspond to spatial clusters, since cell-cell junctions are stable and neighbours are not exchanged over time.

Summarised, we find regular proliferation at low cell densities, i.e. for $1 \frac{10^3}{mm^2} < \rho < 3 \frac{10^3}{mm^2}$, reflected by the regular distances between the peaks in Fig. 2.3 B. At the density $\rho \approx 5, 5 \frac{10^3}{mm^2}$ or during generation 9, respectively, CIP sets on (Fig. 2.1), leading to a broadening of the CCD (Fig. 2.2). In the following section we describe a model providing a test for our understanding of the MDCK's proliferation behaviour at low cell densities.

2.3. Model for free proliferation

We introduce a model for cell proliferation in the low-density regimes ($1-2 \frac{10^3}{mm^2}$), assuming Gaussian-distributed cell cycle periods in absence of CIP. We obtain a mean μ and standard deviation σ of the cycle times T by fitting

$$p(T) = \frac{1}{\sigma\sqrt{2\pi}} e^{-\frac{(T-\mu)^2}{2\sigma^2}} \quad (2.1)$$

to the cell cycle times found in the corresponding density regime. We obtain $\mu = T_0 \approx 20h$ and $\sigma \approx 3h$ (Fig. 2.4).

According to this model we can estimate the number of generations g^* after which cells belonging to different generations are expected to overlap, i.e. their divisions occur at the same time:

$$g^* \approx \frac{\mu}{\sigma} \approx \frac{20h}{3h} \approx 6, 7 \quad (2.2)$$

To test our model for free proliferation in the low-density regime, we simulated the age distributions and mitosis densities and compared them to the values derived from the experimental data.

In Fig. 2.5 we see the simulation results of our Gauss-model for free proliferation, which is capable of describing the cell age distributions for the density regimes of

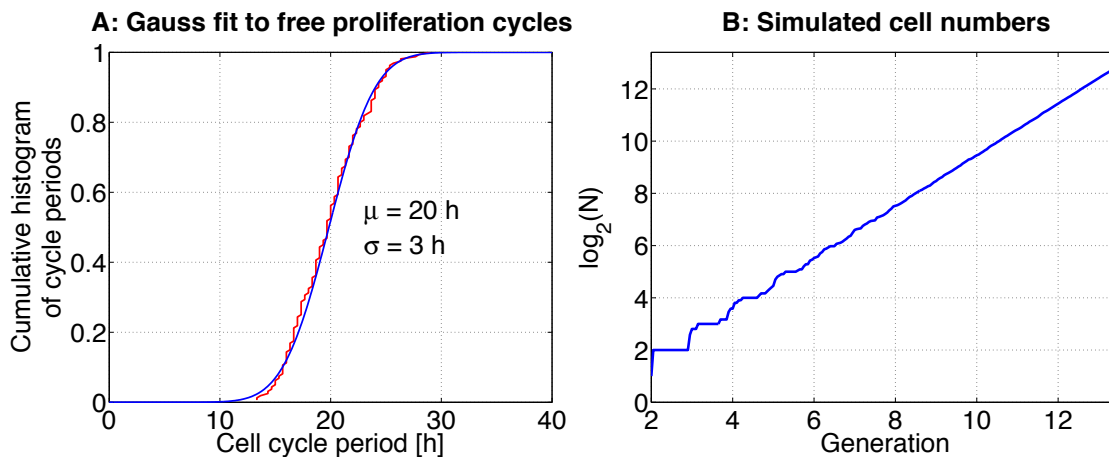


Figure 2.4.: Gaussian distribution fit to cell cycle data in the free proliferation regime. A: Cumulative histogram of cycle periods (red) and Gaussian fit function (blue). B: Simulated cell numbers start increasing exponentially in a stepwise manner (cf. Fig. 2.1), before cells desynchronize and growth becomes homogeneous.

maximal proliferation, i.e. up to a density of $3 \frac{10^3}{\text{mm}^2}$ or generation 9, respectively. Comparing the results shown in Fig. 2.3 and Fig. 2.5, we see good agreement of theory and experiment for the proliferation patterns in the low-density regime.

Using different data sets we could visualise the critical generation number g^* , from which on there are no more mitosis-free gaps between succeeding generations of cells, cf. Fig. 3.3.

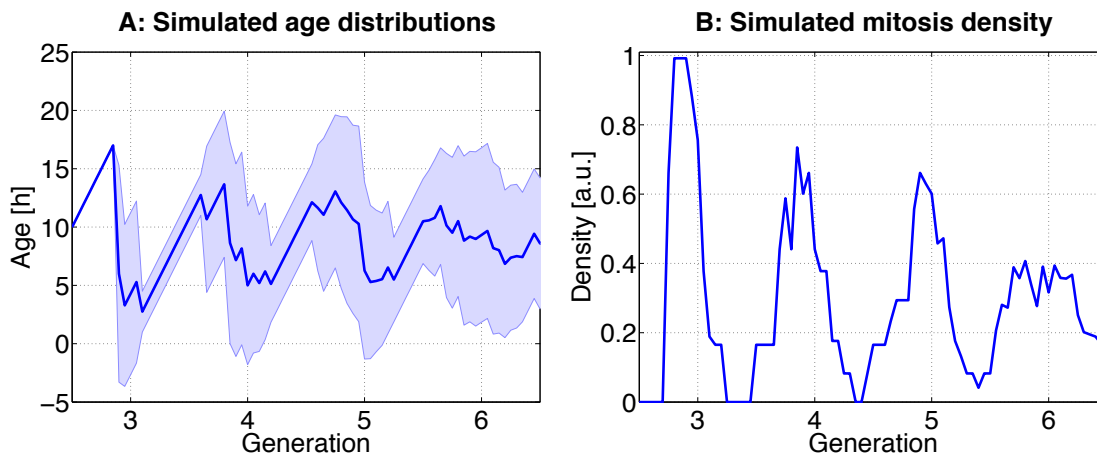


Figure 2.5.: Simulated data. A: Mean (line) and standard deviation (band) of cell age distributions. The distribution gets broader as the cells increasingly desynchronize until the distribution becomes stationary (cf. Fig. 2.6 B). B: Spatiotemporal mitosis density, resembling a damped oscillation (cf. Fig. 2.3).

Fig. 2.6 A shows the damped oscillating behaviour of mean and standard deviation of the cell age distribution predicted by our model under the assumption that CIP has not set in yet. Consequently the model also predicts that for $g \gg g^*$ the age distribution asymptotically reaches a steady state; this age distribution can be interpreted as the probability distribution for future cell divisions (Fig. 2.6 B). It shows high probabilities for short waiting times and low probability for long waiting times and - to this extent - resembles a Poisson distribution, which represents the waiting time for completely uncorrelated chance events. However, in our experimental setting, CIP sets in around generation 9, thus preventing a measurement of this stationary age distribution.

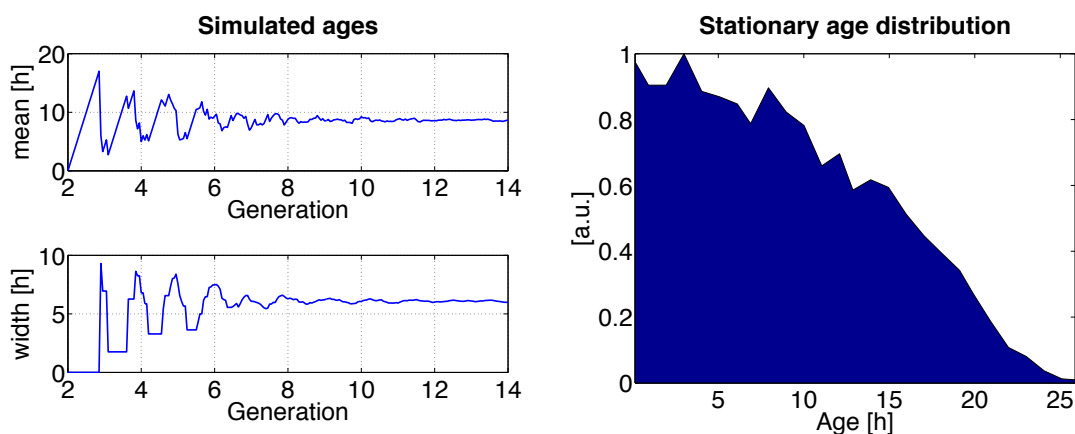


Figure 2.6.: Asymptotic stationary age distribution. A: Mean and standard deviation of simulated cell age distributions, same as in Fig. 2.5 A, but shown until constant values are reached. B: Corresponding simulated age distribution at generation 14.

2.4. Cell cycle heterogeneities

We also wanted to test for the hypothesis that asymmetric cell divisions would lead to unequal division times in sister cells. Asymmetry can arise, for example, from the unequal distribution of cytoplasm or metabolic components among daughter cells. Assuming that cells have to grow until they reach a critical cytoplasmic mass or a critical level of a cell cycle regulator before they can go through another round of cell division, the daughter cell that receives less cytoplasmic material would take longer to synthesize the required components.

Therefore, we define a measure for the relative difference in cell cycle periods in sister cell pairs and random cell pairs (born within the same 90 minutes), where T_i

and T_s are the cycle periods of the slower and the faster dividing cell, respectively:

$$d_r(T_l, T_s) = \frac{T_l - T_s}{(T_l + T_s)/2} \quad (2.3)$$

Fig. 2.7 shows approximately 20 % difference in division times between sister cells in all density regimes. The relative difference between random pairs on the other hand closely resembles the increase in the CV of the cell cycle distribution, which was measured as a function of cell density (see inset in Fig. 2.2 B). The columns in the highest density regime are likely to be distorted due to the cut-off in experiment time.

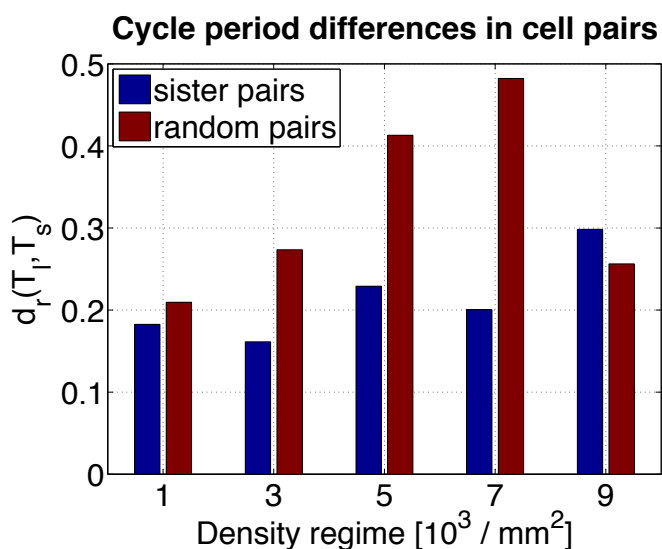


Figure 2.7.: Sister vs. random cell pair cycle differences, binned by density regime. Sister cells show a similar difference of about 20% in all density regimes, whereas random cell pairs show increasing differences as a function of increasing cell density. The lower difference at the highest density should not be taken into account, since here very long cycle periods are not represented due to the cut-off in experiment time.

The heterogeneity in random cell pairs can be explained by density heterogeneities emerging in the medium density regime ($3-7 \frac{10^3}{\text{mm}^2}$), see Fig. A.2. We observed clusters of different densities, which lead to differences in cell cycle duration as one would expect from the cell area-dependence of division times. In contrast to random pairs, sister cell pairs reside preferentially in the same density cluster, since they are neighbours, and thus have similar cell cycle times.

2.5. Conclusion

We conclude that the Gauss-model for free proliferation, which describes cell cycle progression like a regular inner clock, is appropriate as long as CIP does not set on, i.e. in our data for 9 generations or up to a cell density of $\rho \approx 5, 5 \frac{10^3}{mm^2}$, respectively. The desynchronisation of cell cycles in a cell colony derived from a common ancestor cell becomes significant after 6 generations of cell divisions and is further accelerated by the broadening of the CCD due to CIP. This desynchronisation of cell divisions is thought to facilitate the morphogenesis of a regular epithelial tissue, once the transient states of density heterogeneities are passed. For the absence of CIP a stationary age distribution is predicted by our model. In the medium density regime, i.e. $3 \frac{10^3}{mm^2} < \rho < 7 \frac{10^3}{mm^2}$, sister cells still behave similar in terms of proliferation rates, but random pairs of cells having possibly different environments, exhibit a greater diversity.

3. Migration and proliferation

For our second project, presented in this section, we analysed the influence of synchronous cell divisions on the collective migration behaviour of young colonies.

3.1. Growth and motility dynamics

In epithelial morphodynamics, motility decreases first as cellular density increases, followed by the decrease of proliferation (sec. 1.3). We first set out to establish a model system that is capable of reproducing these findings by allowing for quantitative measurement of growth and motility by single cell tracking.

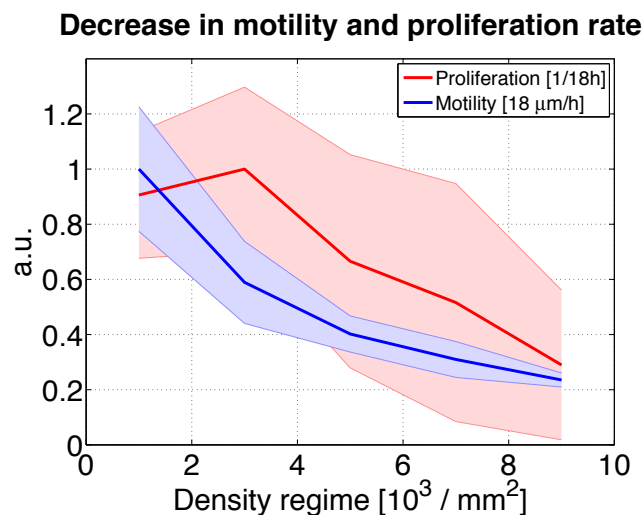


Figure 3.1.: Relative motility (blue), followed by proliferation rate (red) drop down to a third of their initial values while cell density increases by one order of magnitude. This transition occurring during 2 weeks of *in vitro* tissue growth reflects a MET.

In Fig. 3.1 the maximal value on the ordinate, i.e. a proliferation rate of $(18h)^{-1}$ or a motility of $18\mu\text{m}/\text{h}$, represents the mesenchymal-like phenotype of the MDCK-2 cells, as found at low cell density and optimal growth promoting conditions (cf. chapter 5, cell culture). At high cell density instead, the proliferation rate decreases due to CIP (cf. previous chapter) and motility drops dramatically, which reflects the

epithelial phenotype. This mesenchymal-epithelial transition (MET), coincides with the onset of physiological tissue functionality (evident in the emergence of domes, sec. 2.1) and the transition from tissue growth to homeostasis.

For the following investigation we consider the low density regime of free proliferation and maximal motility, i.e. $\rho < 3 \frac{10^3 \text{ cells}}{\text{mm}^2}$.

3.2. Migration patterns of young colonies

At low densities, where the MDCK cells have the ability to migrate with their maximal speed, but have already established stable cell-cell junctions, they show the tendency to migrate in circles around their common central point, which leads to a rotation of the whole colony.

We quantify this behaviour by calculating the mean angular velocity of the colony:

$$\vec{\omega}(t) = \frac{1}{N_{\text{cells}}(t)} \sum_{i=1}^{N_{\text{cells}}} \frac{\vec{r}_i'(t) \times \vec{v}_i'(t)}{|\vec{r}_i'(t)|^2} \quad (3.1)$$

Fig. 3.2 A shows the z-component of $\vec{\omega}(t)$ for a typical colony; obviously this is the only non-zero component, since our cell culture system lives on a 2-dimensional surface. The sign of ω_z reflects the sense of rotation and the decreasing amplitude displays the decline of coherent rotatory migration as the colony grows.

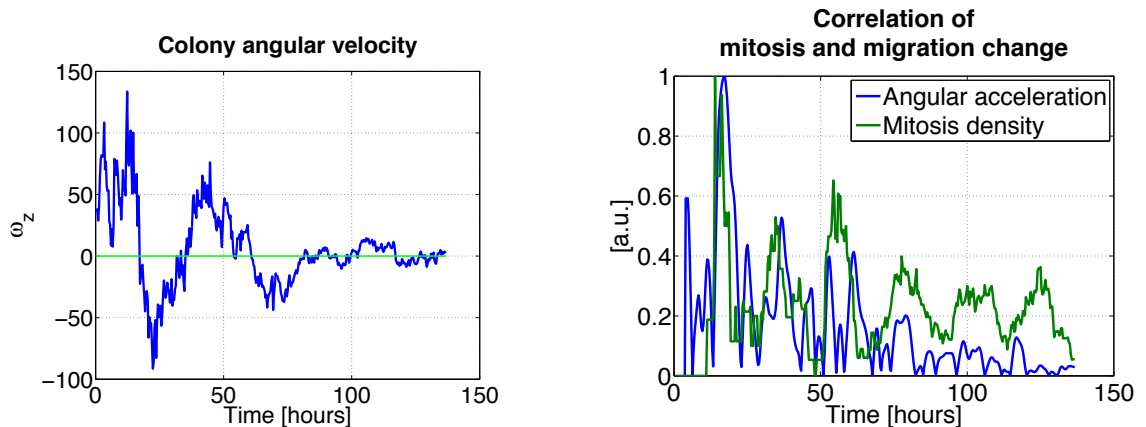


Figure 3.2.: A: Mean angular velocity of a typical colony (eq. 3.1) with decreasing amplitude and oscillating sense of rotation (represented in the sign of ω_z). B: Correlation of mitosis density and change in angular velocity is significant for about 4 rounds of cell divisions (green peaks), which is the number of clear zero-crossings in A.

Interestingly, the period of changes in the sense of rotation of the colony resembles the cell cycle period in this density regime, i.e. 20 h, suggesting a possible causal relation between the two.

By comparing the mitosis density and the temporal derivative of this colony angular velocity, we find a strong correlation of these two parameters that lasts over several generations (see Fig. 3.2 B). This indicates that as long as the mitosis density, i.e. the fraction of cells that divide simultaneously, is sufficiently high, an overthrow of the collective migration pattern can occur. In the following section we will further analyse the connection between cell divisions and direction changes in cell migration.

Fig. 3.3 shows the normalised squared colony angular velocity (in order to display only its relative amount) and the normalised mitosis density, respectively, averaged over 9 colonies after aligning the data by their logarithmic cell numbers used for defining the generation number. After 7 generations, the colony is still located in the free proliferation regime, i.e. $\rho < 3 \cdot 10^3 \text{ mm}^{-2}$ (cf. Fig. 2.1, day 5). Therefore the strong decrease of coherent angular velocity as shown in Fig. 3.3 A cannot be explained by a general decrease in cellular motility, but seems to be due to less correlation in the migration of the cell collective. The mitosis density plotted in Fig. 3.3 B nicely confirms the significant overlap of mitoses belonging to different generations from a critical generation onward, which we calculated earlier to be $g^* \approx 6,7$ (cf. eq. 2.2).

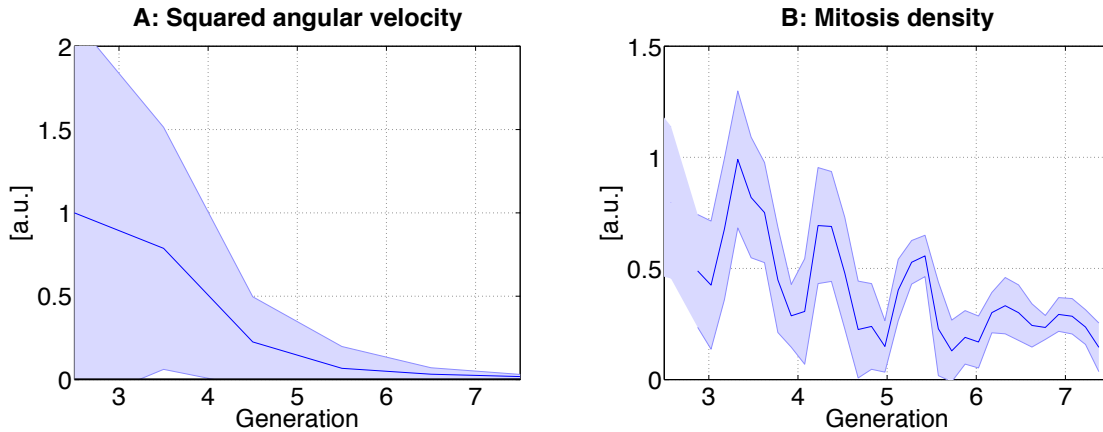


Figure 3.3.: Summary over 9 colonies, aligned according to generation numbers, which are defined by the logarithmic cell number (1 generation $\hat{=}$ 20h). Mean (line) and standard deviation (band) of squared colony angular velocity (A) and mitosis density (B).

3.3. Dissecting changes in direction

To better understand how cell migration changes during mitosis, we studied the direction of migration and its angle between mother and daughter cells and between two sister cells, respectively. Furthermore, we analysed the direction of migration of two sister cells with respect to the division axis of the mitosis they arose from. Finally, we measured the global orientation of division axes with respect to the whole colony. The angles were calculated between pairs of vectors obtained by averaging speed vectors over the first (for daughters) and last (for mothers) few time points of tracked migratory paths.

We found a strong correlation in the migration directions of daughter cells. This provides evidence that sister cells have a strong preference to migrate in parallel along same tracks (Fig. 3.4 A). In contrast, migration directions of mother cells and their respective daughter cells are uncorrelated (Fig. 3.4 B). This finding supports the idea that cell division can interrupt previously established patterns of migration and enable the emergence of new ones.

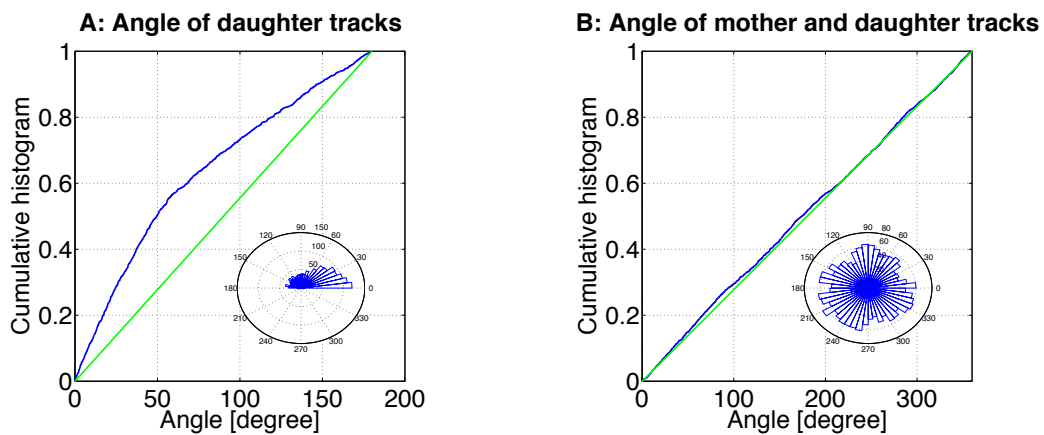


Figure 3.4.: Angles between the migration directions of sister cell pairs (A) and mother-daughter cell pairs (B). Sister cells preferentially migrate in parallel, whereas the path of the mother cells is not preserved after mitosis.

Furthermore, we find a slight preference of the division axis to be aligned with the migration direction of the mother cell (not shown) and a slight preference of daughter cells to begin their migration along the division axis of the mitosis that generates them (see Fig. 3.5 B).

On the global level, the division axis is preferentially oriented tangential to the colony border, consistent with the observation that cells tend to divide along their migration direction.

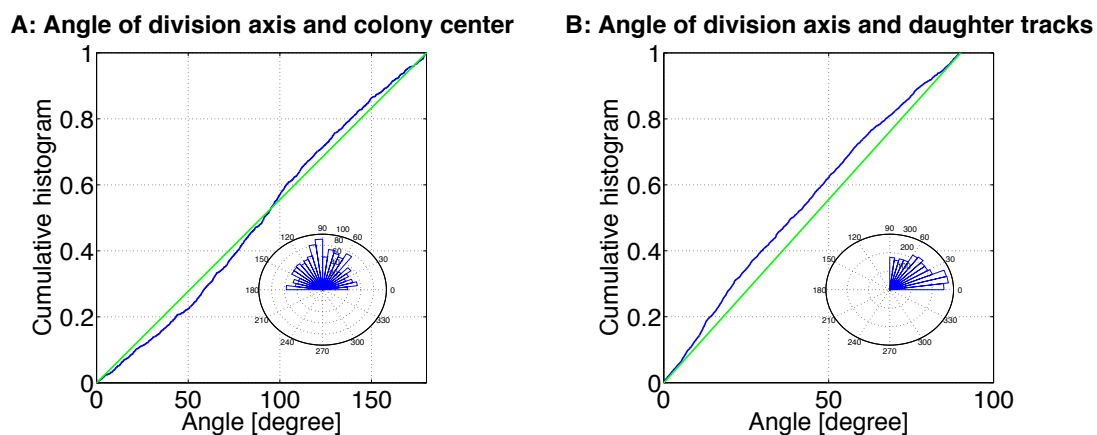


Figure 3.5.: Division axis orientation. A: Global orientation of division axes respective the centre of the colony, preferentially tangential to the border of the colony. B: Initial daughter migration preferentially along their division axis.

3.4. Conclusion

Our findings strongly support the idea that highly synchronous cell divisions, as they occur in the low density regime of young MDCK colonies, can have a dramatic effect on collective migration patterns. If not drowned out by other mechanisms regulating cellular behaviour, they lead to a disruption of previously established patterns of migration, whereupon cells may adopt very different directions of migration.

However, in tissue morphodynamics this most likely holds true only for the temporary phase of low density, high motility and regular proliferation, which by default leads to its own arrest, i.e. higher density, less motility and the inhibition of proliferation.

4. Summary & Discussion

In this thesis we investigated cell cycle correlations in epithelial tissue development. We characterised the proliferation behaviour of MDCK-2 cells as they grew from low ($\rho \approx 1 \frac{10^3}{\text{mm}^2}$) into high ($\rho \approx 11 \frac{10^3}{\text{mm}^2}$) cell densities. We observed that during this process first the cellular motility starts to drop (overall from $20 \frac{\mu\text{m}}{\text{h}}$ to $5 \frac{\mu\text{m}}{\text{h}}$), followed by the decrease in proliferation due to contact inhibition of proliferation (CIP), setting in at $\rho \approx 5,5 \frac{10^3}{\text{mm}^2}$. Further we observed the emergence of domes at a cell density of $\rho \approx 6,5 \frac{10^3}{\text{mm}^2}$, reflecting a transition in biological function. We found regular proliferation at low cell densities, i.e. for $1 \frac{10^3}{\text{mm}^2} < \rho < 3 \frac{10^3}{\text{mm}^2}$, describing a Gaussian-distribution of cell cycle periods with a mean $\mu = 20$ h and a standard deviation of $\sigma = 3$ h. This behaviour was predicted by our model for free proliferation and confirmed experimentally. Moreover, our model predicted a stationary age distribution for generations $g \gg 6,7$. We found no significant asymmetries between sister cells ($d_r \approx 20\%$ independent of cell density), but found that random cell pairs exhibit increasingly diverse cycle periods as cell density increases. Furthermore, we described the collective rotative migration behaviour of young, small colonies of MDCK-2 cells. Their migration is correlated for about 6 generations, corresponding to a cell number $N = 64$. At the same time, cell cycle correlations are diminished so far, that different generations are no longer separated by temporal clusters of mitoses, but intermingled. We observed that the collectively migrating colonies change the sense of their rotation in correlation with the occurrence of highly synchronised mitoses, indicating that cell divisions perturb the migration patterns. This hypothesis was supported by the finding that motions of daughter cells are highly correlated, whereas mother and daughter paths are completely uncorrelated.

Our measurement of CIP the MDCK-2 cells is consistent with earlier work by Castor (1972), which showed that the decrease in cellular motility precedes the decrease in proliferation in epithelial-like cell lines, cf. Fig. 3.1. For the onset of CIP we found a critical cell area $A_c \approx 180 \mu\text{m}^2$ (corresponding to the critical cell density of $\rho \approx 5,5 \cdot \frac{10^3}{\text{mm}^2}$, Fig. 2.1) which does not contradict $A_c \approx 200 \mu\text{m}^2$, found by Puliafito *et al.* (2012), provided that MDCK cells grow into different densities depending on the stiffness of the substrate. The decrease of motility from 20 to $5 \frac{\mu\text{m}}{\text{h}}$ is also in good agreement with Castor (1972), Petitjean *et al.* (2010) and Puliafito *et al.* (2012).

Biologically, it would be interesting to correlate these phenomenological transitions in physical parameters with molecular markers for mesenchymal and epithelial sig-

nalling pathways, to show a connection between physical and biological phenotypes. So far we can only rely on the emergence of domes as a read-out for a switch in biological function (sec. 2.1).

The idea that freely proliferating cells follow an internal clock of finite precision is supported by our observations of a growing MDCK colony over a few generations until CIP sets in. A mutant cell line lacking the CIP phenotype will be informative in the future to further test our model of free proliferation and compare it to the results of Chiorino *et al.* (2001), e.g. in regard to the predicted steady state age distribution.

Simple mathematical models of tissue growth often assume that cell divisions follow a Poisson process of uncorrelated chance events [Lars Hufnagel, personal communication]. According to our findings, this is only appropriate where the width of a distribution of division times approximately equals its mean, $\sigma(T) \approx \mu(T)$, and in situations where phenomena such as CIP do not play a significant role. In this case, the age distribution would quickly become stationary and could be interpreted as the probability distribution for future cell divisions, cf. Fig. 2.6.

We view the onset of CIP as a growth control feedback from the tissue scale, where cell density is defined, to the sub-cellular scale, where the regulating pathways act locally, cf. Shraiman (2005). The actual molecular mechanism, though, was not addressed in this work.

A possible scenario is that the degree of synchronicity in cell cycles impacts on the final cell density of a tissue. Since the restriction checkpoint is passed some hours before cells divide, this would lead to an earlier inhibition of proliferation in cases where neighbouring cells divided earlier. If, for instance, 100 cells are able to pass the restriction point simultaneously, this might not happen if 50 of them doubled earlier, therefore increased the density and potentially inhibited the passing of all the rest, leading to a lower final cell number and therefore a lower cell density. However, there is no evidence that such a difference in final density would have a biological relevance. See sec. A.3 for a preliminary experiment related to this consideration.

Asymmetric cell divisions between sister cells, if at all they exist in MDCK-2 cells, seem to have no significant impact on division times. Rather local cell density or mechanic stresses felt by the cells via their mechanosensitive machineries are expected to determine cell cycle regulation (at least in the absence of other regulating mechanisms such as morphogen gradients). This way we explain the cell cycle heterogeneities in Fig. 2.7, which resemble the CV in the inset of Fig. 2.2 B. Random cell pairs, in contrast to sister cell pairs, are likely to reside in greater distances and therefore in clusters of different densities leading to differently regulated cell cycle periods, see also Fig. A.2. This fits to an also occurring velocity heterogeneity as cell density increases, as described by Angelini *et al.* (2011).

From the velocity correlation length for MDCK cells, which Petitjean *et al.* (2010) measured to be $200\mu\text{m}$, we can estimate a number of cells that are able to coordinate their migrations. We measured a standard cell density of $\frac{10^3}{\text{mm}^2}$, which corresponds to

a cell radius of $32\mu m$. This means that in two dimensions 39 cells will have the tendency to correlate their migrations, if they are as strongly coupled as MDCK cells. This cell number is reached just after five generations of cell divisions, which approximately matches our observation of colony sizes when the colony stops rotating (Fig. 3.3 A).

Our observation of collectively rotating MDCK cells on a free glass surface can be compared to the setup of Huang *et al.* (2005), who analysed the rotations of pairs of cells on micropatterned substrates. This study reports spontaneous changes in the migratory direction dependent on the persistence time of the cells random-walk behaviour, but independent of cell divisions, which appeared to be the determining factor in our case. A future experiment to further investigate rotating colonies will include an inhibitor of cell proliferation to test the hypothesis that it is mitosis that causes the changes in direction of migration.

Considering the dramatic events occurring inside a cell during mitosis [Théry & Bornens (2008)] it is no surprise that cells do not maintain their migration patterns if not supported by neighbouring cells without ongoing mitosis. Solely because of the multiple functions of the microtubule organising centre during cell migration and cell division, these processes are unlikely to be independent of each other.

We conclude that cell cycle correlations in epithelial tissue morphogenesis have their origin in cell cycle distributions with their mean value being much greater than their width, $\mu(T) \gg \sigma(T)$, and are desynchronised by two independent mechanisms. One consists of a trivial broadening of mitosis distributions from one generation to the next. The other one arises from a broadening of the cell cycle distribution due to contact inhibition of proliferation at high cell density. We propose that this desynchronisation of cell cycles facilitates the emergence of a regular epithelial tissue.

5. Materials & Methods

Fluorescent MDCK-2 cell line

For this work we used two different fluorescently labelled subclones of the cell line MDCK-2 (ATCC Number: CRL-2936):

MDCK-2 Fucci (clone 6a)

was produced by subsequent infection with pseudotyped HIV-1-derived lentivirus encoding mAG-hGem(1-110) and mKO2-hCdt1(30-120), the two components of the fluorescent ubiquitination-based cell cycle indicator Fucci (Fig. 5.1) [Méchali & Lutzmann (2008), Sakaue-Sawano *et al.* (2008)]. Both Fucci markers are expressed from a human EF1alpha promoter. After infection, cells were clonally sorted by FACS based on expression of the respective fluorescent signals, and were characterised by live cell time-lapse imaging.

MDCK-2 H2B-mCherry (clone 2)

was generated as described above by infection with lentivirus encoding the human histone 2B tagged with mCherry (H2B-mCherry) expressed from a human PGK promoter.

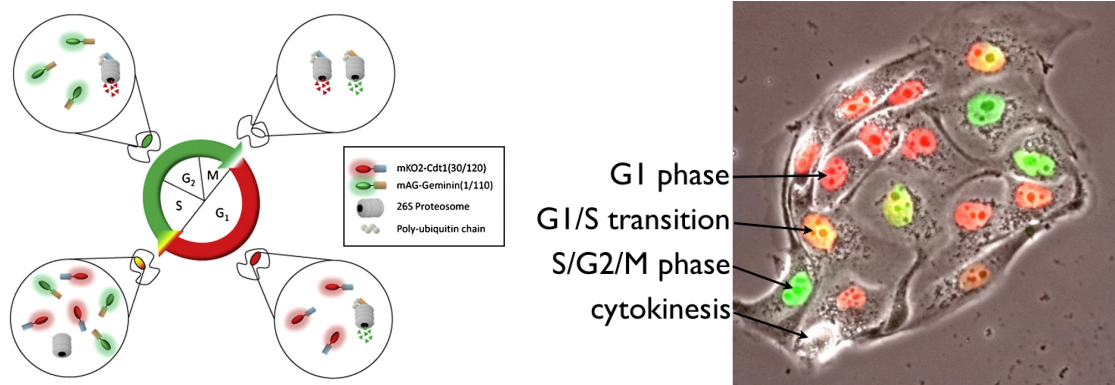


Figure 5.1.: Left: The concept of the fluorescent ubiquitination-based cell cycle indicator (Fucci) [Newman & Zhang (2008)]. Right: Typical MDCK-2 Fucci cells imaged using our microscopic setup (see below). As indicated, four stages of the cell cycle are separable.

Cell culture

Cells were cultured using MEM growth medium, containing 90% (v/v) Minimum essential medium (MEM, Sigma-Aldrich) and 10% (v/v) Fetal bovine serum (FBS, A10109-0878, PAA), at 37°C and 5% CO₂ in 75 cm² flasks (Greiner bio-one).

For live cell imaging, we used medium, containing 88% (v/v) MEM without phenol red (Sigma-Aldrich) supplemented with 2,2 g/l NaHCO₃, 10% (v/v) FBS, 1% (v/v) 200 mM L-Glutamine (Gibco) and 1% (v/v) P/S (Penicillin/Streptomycin 100x solution, Sigma-Aldrich).

Imaging

Cells were seeded in 3,5 cm glass bottom dishes (WillCo) at densities of 10² to 10⁵ cells per dish and mounted into a custom-made microscopy chamber for stable gas conditions. The chamber was sealed with Baysilone silicone paste (GE Bayer Silicones), mounted onto the heated microscope and connected to the gas supply. Imaging started about one day after seeding, so that cells at most had settled down and started proliferation.

We used a UPlanApo 20x/NA0.70 objective (Olympus Deutschland) and the Andor iQ software (V1.10.5, Andor Technology) at a customized microscope consisting of an IX-81 microscope (Olympus Deutschland), an automated stage (Märzhäuser Wetzlar), a spinning disc unit (Yokogawa Europe), and an iXon 3 897 EMCCD camera (Andor Technology). For excitation, solid-state lasers emitting at 491 nm and 562 nm were used.

Images were taken every 20 or 30 minutes for about one week in each case. The medium was changed daily, as the freshness of the medium had a strong influence on the motility of cells (sec. A.1).

Image analysis

Preprocessing of the microscopic images involved a maximum projection, since several z-planes were taken to minimise the data lost due to cellular nuclei out of focus. Several fields of view were stitched to enable the tracking of cells over several days. Background was corrected by subtraction of the morphologically opened image from the original one.

For image segmentation we used the classification-based trainable image segmentation toolkit *ilastik*, developed by Sommer *et al.* (2011), followed by self-written Matlab algorithms, to interpret the obtained probability maps for segment classes, sizes, and positions. Fig. 5.2 shows typical data, training, and segmentation results.

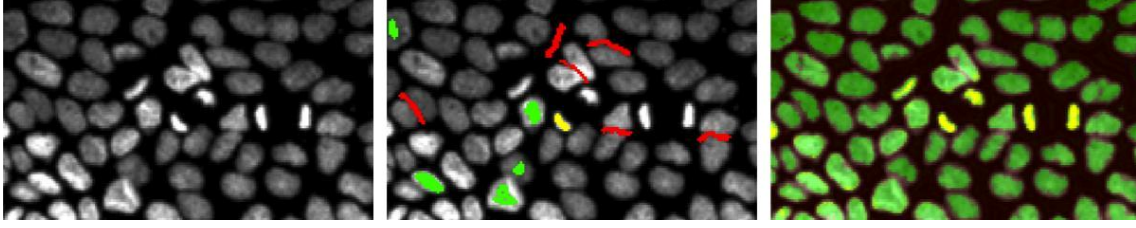


Figure 5.2.: Using the Ilastik toolkit [Sommer *et al.* (2011)] for trainable local classification-based image segmentation. Left: Z-projected and background-corrected MDCK-2 H2B data. Middle: Training for the classification of background (red), interphase (green) and mitotic nuclei (yellow). Right: Resultant segmented nuclei belonging to interphase (green) or mitotic phase (yellow), respectively.

Via voronoi tessellation of the segmented cells' centre of masses [Honda (1978)] we obtained an approximation for the corresponding cell areas. We calculated cellular densities by taking the inverse of the mean cell area at every time point.

For an estimation of the cellular motilities, at first an optical flow field was calculated for each two succeeding images using an algorithm developed by Liu (2009). Subsequently cells were tracked over time minimising the cost function ϕ , which takes into account the centres of mass \vec{r} of nuclei i and j of two succeeding time-points, flow field estimates $\Delta\vec{r}$, cell areas a and class probabilities p as obtained from the segmentation process with scaling factors c_a and c_p :

$$\phi_{i,j} = (\vec{r}_i + \Delta\vec{r}_i - \vec{r}_j)^2 + c_a \cdot (a_i - a_j)^2 + c_p \cdot (p_i - p_j)^2 \quad (5.1)$$

Fig. 5.3 (top) shows single cell tracks for several time points on top of the MDCK-2 H2B data at low and at high cell density, respectively. Mother daughter cell relations (indicated by white bars) were assigned using a self-written semi-automated graphical user interface in Matlab, from which we also obtained cell lineages (bottom).

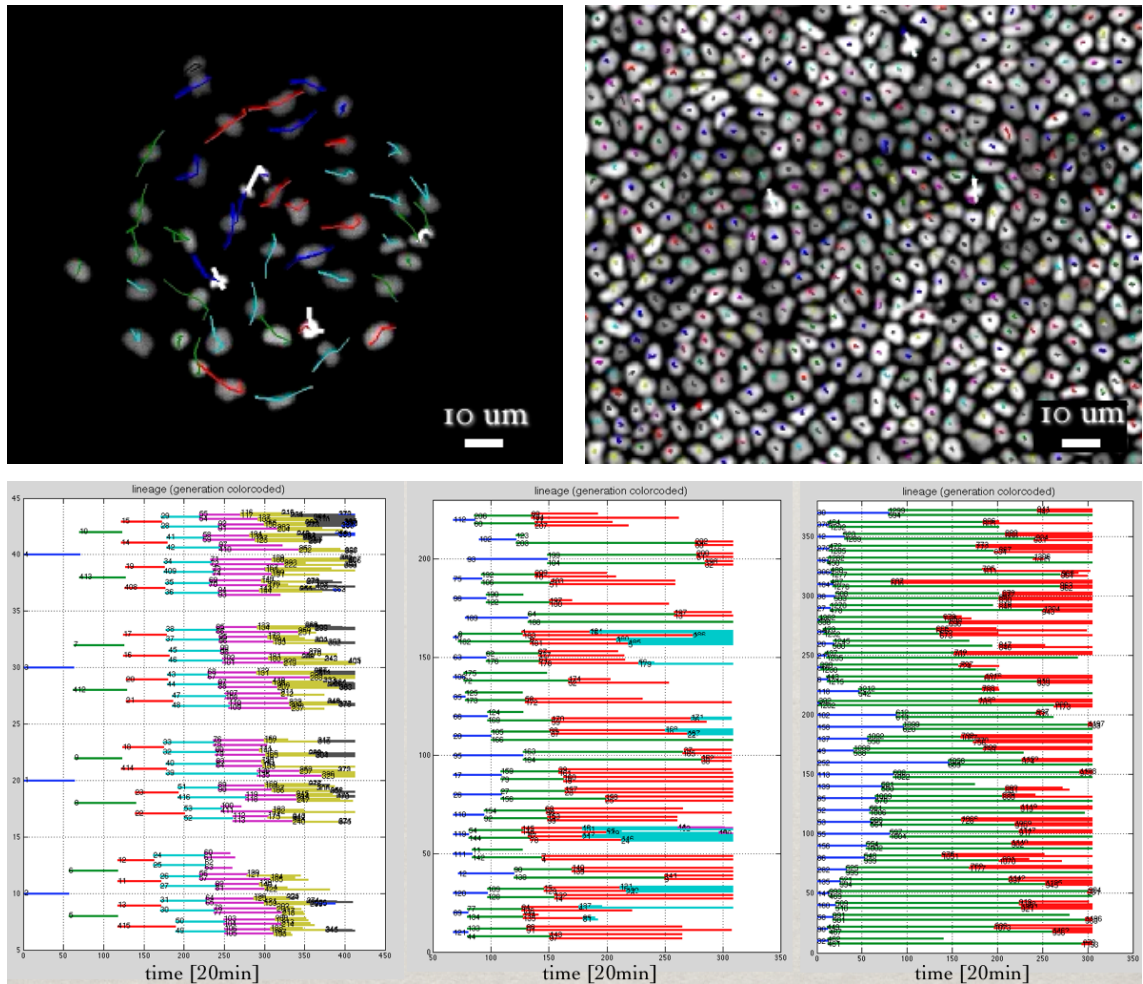


Figure 5.3.: Top: Single cell tracks at low (left) and high (right) cell density on top of the MDCK-2 H2B data. Positions at several time points are shown by the coloured lines. Family relations are colour-coded. White bars indicate mitoses. Bottom: Cell lineages at three different densities with generations colour-coded.

A. Appendix

A.1. Medium sensitivity

To test for the medium sensitivity of the MDCK-2 cells, we measured their motility at different cell densities. Fig. A.1 shows that in case medium was renewed every third day the motility drops already at lower densities, i.e. larger cell areas, due to the degradation of some ingredients. A daily medium renewal ensured stable conditions for cell motility and assumably also for the proliferation behaviour.

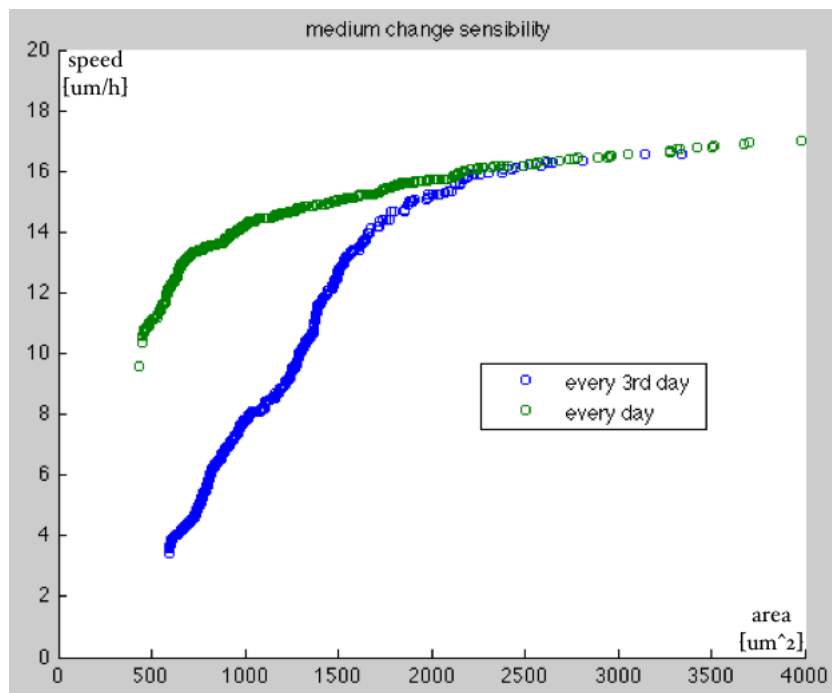


Figure A.1.: Medium sensitivity of cellular motility.

A daily medium renewal ensured stable conditions for cellular motility; in contrast, a medium renewal only every third day led to decreased cellular motility already at lower cell densities, i.e. larger cell areas.

A.2. Density fluctuations

The medium cell density regime of developing MDCK-2 colonies, i.e. $3 \frac{10^3}{\text{mm}^2} < \rho < 7 \frac{10^3}{\text{mm}^2}$, is characterised by density heterogeneities. Fig. A.2 shows some preliminary results demonstrating that in this regime we find clusters of different densities. Cells in a local environment of higher density are expected to have prolonged cell cycle times. This explains the cell cycle differences as described in Fig. 2.7. In future experiments the expression of molecular markers known to be associated with the mesenchymal-epithelial transition should be correlated with local cell density to prove our hypothesis that clusters of increased cell density display seeds of cell differentiation.

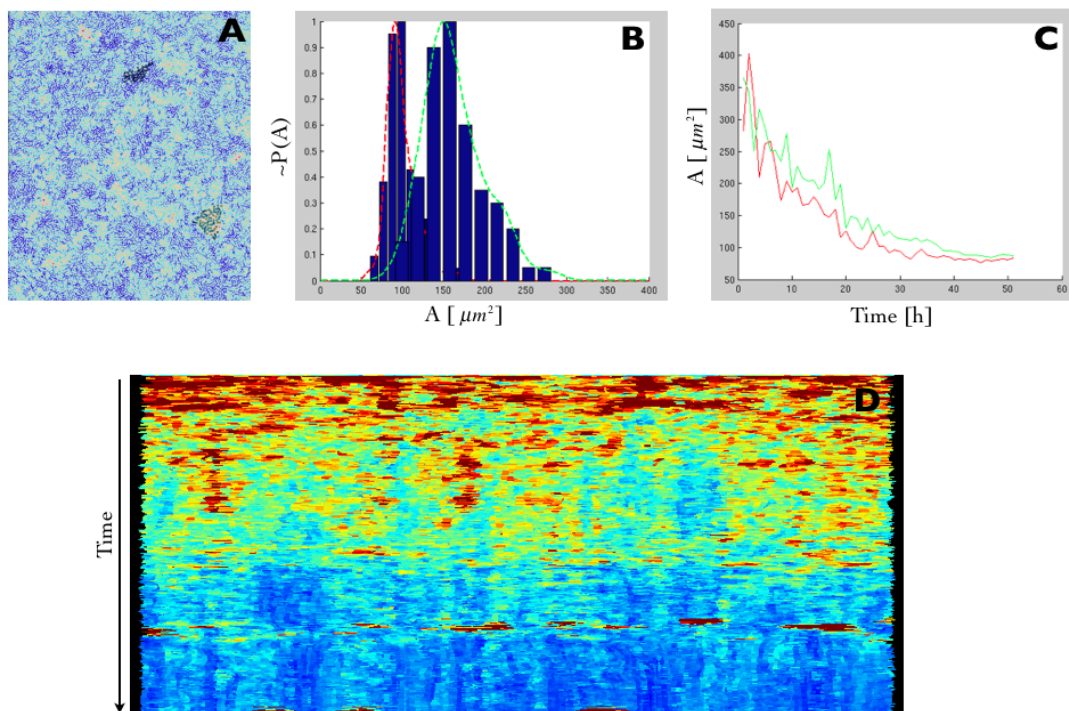


Figure A.2.: Density heterogeneities. A: Segmented MDCK-2 center of masses with cell area colour-coded (blue: small cell area, red: large cell area). Two regions of interest of relatively low and relatively high cell density. B: Cell area distributions of the regions selected in A. C: Temporal evolution of the mean cell area of cells located in the regions selected in A. During the first 8 hours they cross, afterwards both values shrink and converge towards a constant high density. D: Kymograph of the tissue with cell areas colour-coded (red...blue $\hat{=} A = 2000 \dots 100 \mu\text{m}^2 \hat{=} \rho = 0,5 \dots 10 \frac{10^3}{\text{mm}^2}$). We see the clustering in space and time of cells having similar areas and how these converge towards a homogeneous high density. Also the emergence of domes in the later third is apparent twice in simultaneously arising red spots which reflect the fact that cells in the dome are not detected, so that the neighbouring cells seems to have larger areas.

A.3. Spatially constrained tissues

The motivation for this preliminary experiment was to use a mechanical constraint to accelerate the process of CIP. For this we designed a PDMS membrane with holes of different diameters. The membrane was placed on a glass bottom dish. MDCK-2 Fucci cells were plated into the holes of available space at a density below confluence and the usual imaging medium was applied. The Fucci cell cycle marker (Fig. 5.1) allowed for a simple readout of cell proliferation on the tissue scale by counting the fraction of cells in S/G2/M phase.

Interestingly, cells in wells having a diameter of $400\mu m$ and smaller appeared to go into CIP faster, i.e. at lower cell densities, compared to the cells of unconstrained colonies (Fig. A.3).

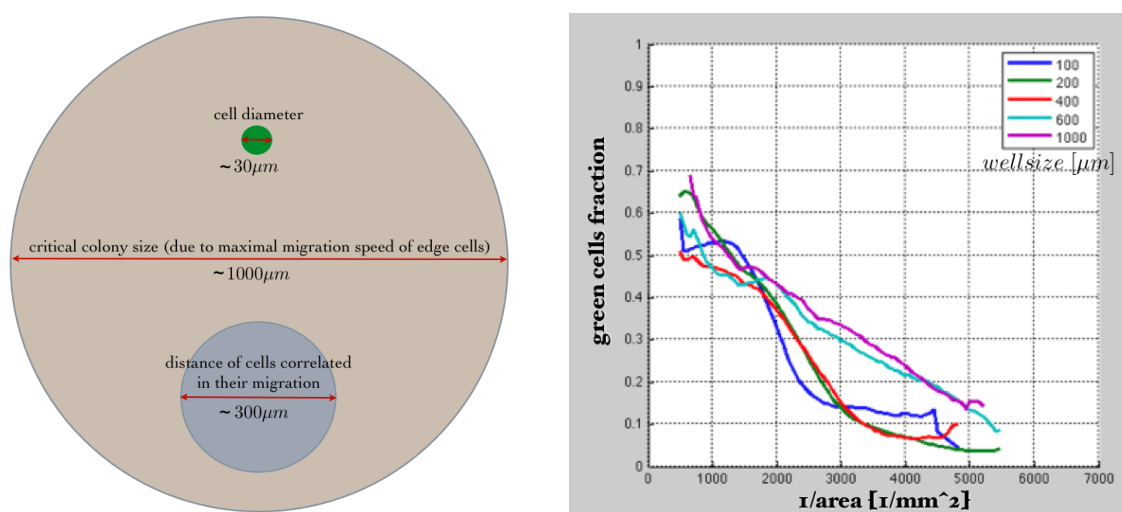


Figure A.3.: Wellsizedependent proliferation behaviour.

Left: Schematic experimental setup based on different scales estimating cell diameter, correlation length, and critical colony size expected to resemble the unconstrained situation. Right: Preliminary results showing the cell density-dependent proliferation behaviour of colonies in wells of different diameters. Cells in wells having a diameter of $400\mu m$ and smaller show an increased CIP already at lower cell densities.

Possible explanations for the observed phenomenon include differences in the mechanical environment due to the different ratio of border to area or simply an artefact due to the suboptimal performance of the experimental setup. Furthermore an influence of cell cycle correlations on this phenomenon can not be excluded.

Bibliography

- Abercrombie, M, & Heaysman, J E. 1953. Observations on the social behaviour of cells in tissue culture. I. Speed of movement of chick heart fibroblasts in relation to their mutual contacts. *Experimental cell research*, **5**(1), 111–131. PMID: 13083622.
- Abercrombie, M, & Heaysman, J E. 1954. Observations on the social behaviour of cells in tissue culture. II. Monolayering of fibroblasts. *Experimental cell research*, **6**(2), 293–306. PMID: 13173482.
- Aegerter-Wilmsen, Tinri, Aegerter, Christof M, Hafen, Ernst, & Basler, Konrad. 2007. Model for the regulation of size in the wing imaginal disc of *Drosophila*. *Mechanisms of development*, **124**(4), 318–326. PMID: 17293093.
- Alberts, Bruce, Johnson, Alexander, Lewis, Julian, Raff, Martin, Roberts, Keith, & Walter, Peter. 2007. *Molecular Biology of the Cell*. 5 edn. Garland Science.
- Alim, Karen, Hamant, Olivier, & Boudaoud, Arezki. 2012. Regulatory Role of Cell Division Rules on Tissue Growth Heterogeneity. *Frontiers in Plant Science*, **3**(Aug.). PMID: 22908023 PMCID: PMC3414725.
- Angelini, Thomas E, Hannezo, Edouard, Trepat, Xavier, Marquez, Manuel, Fredberg, Jeffrey J, & Weitz, David A. 2011. Glass-like dynamics of collective cell migration. *Proceedings of the National Academy of Sciences of the United States of America*, **108**(12), 4714–4719. PMID: 21321233.
- Arino, O., & Sánchez, E. 1997. A Survey of Cell Population Dynamics. *Journal of Theoretical Medicine*, **1**(1), 35–51.
- Ayala, Francisco José, & Dobzhansky, Theodosius Grigorievich. 1974. *Studies in the philosophy of biology*. University of California Press.
- Balzer, Eric M., Tong, Ziqiu, Paul, Colin D., Hung, Wei-Chien, Stroka, Kimberly M., Boggs, Amanda E., Martin, Stuart S., & Konstantopoulos, Konstantinos. 2012. Physical confinement alters tumor cell adhesion and migration phenotypes. *The FASEB Journal*, **26**(10), 4045–4056.
- Basan, Markus, Risler, Thomas, Joanny, Jean-François, Sastre-Garau, Xavier, & Prost, Jacques. 2009. Homeostatic competition drives tumor growth and metastasis nucleation. *HFSP Journal*, **3**(4), 265–272. PMID: 20119483 PMCID: PMC2799988.

- Basan, Markus, Idema, Timon, Lenz, Martin, Joanny, Jean-François, & Risler, Thomas. 2010. A reaction-diffusion model of the cadherin-catenin system: a possible mechanism for contact inhibition and implications for tumorigenesis. *Biophysical journal*, **98**(12), 2770–2779. PMID: 20550888.
- Baum, Buzz, Settleman, Jeffrey, & Quinlan, Margaret P. 2008. Transitions between epithelial and mesenchymal states in development and disease. *Seminars in cell & developmental biology*, **19**(3), 294–308. PMID: 18343170.
- Benedetti, Fabrizio. 2008. *Placebo Effects*. Oxford University Press.
- Bergstrahl, Daniel T, & St Johnston, Daniel. 2012. Epithelial cell polarity: what flies can teach us about cancer. *Essays in biochemistry*, **53**, 129–140. PMID: 22928513.
- Besson, Sébastien, & Dumais, Jacques. 2011. Universal rule for the symmetric division of plant cells. *Proceedings of the National Academy of Sciences*, **108**(15), 6294–6299.
- Bindschadler, Michael, & McGrath, James L. 2007. Sheet migration by wounded monolayers as an emergent property of single-cell dynamics. *Journal of cell science*, **120**(Pt 5), 876–84. PMID: 17298977.
- Borghi, Nicolas, Lowndes, Molly, Maruthamuthu, Venkat, Gardel, Margaret L, & Nelson, W James. 2010. Regulation of cell motile behavior by crosstalk between cadherin- and integrin-mediated adhesions. *Proceedings of the National Academy of Sciences of the United States of America*, **107**(30), 13324–13329. PMID: 20566866.
- Byrne, Helen, & Drasdo, Dirk. 2009. Individual-based and continuum models of growing cell populations: a comparison. *Journal of mathematical biology*, **58**(4-5), 657–687. PMID: 18841363.
- Cai, L, Hayes, N L, & Nowakowski, R S. 1997. Local homogeneity of cell cycle length in developing mouse cortex. *The Journal of neuroscience: the official journal of the Society for Neuroscience*, **17**(6), 2079–2087. PMID: 9045735.
- Cairns, John. 1975. Mutation selection and the natural history of cancer. *Nature*, **255**(5505), 197–200.
- Castor, Laroy N. 1968. Contact regulation of cell division in an epithelial-like cell line. *Journal of Cellular Physiology*, **72**(3), 161–172.
- Castor, LaRoy N. 1972. Contact Inhibitions of Cell Division and Cell Movement. *Journal of Investigative Dermatology*, **59**(1), 27–32.
- Chiorino, G., Metz, J.A.J., Tomasoni, D., & Ubezio, P. 2001. Desynchronization Rate in Cell Populations: Mathematical Modeling and Experimental Data. *Journal of Theoretical Biology*, **208**(2), 185–199.
- Christiansen, Jason J, & Rajasekaran, Ayyappan K. 2006. Reassessing epithelial to mesenchymal transition as a prerequisite for carcinoma invasion and metastasis. *Cancer research*, **66**(17), 8319–8326. PMID: 16951136.

- Concha, M L, & Adams, R J. 1998. Oriented cell divisions and cellular morphogenesis in the zebrafish gastrula and neurula: a time-lapse analysis. *Development (Cambridge, England)*, **125**(6), 983–994. PMID: 9463345.
- Cooper, Geoffrey M., & Hausmann, Robert E. 2008. *The Cell: A Molecular Approach: 4th (fourth) Edition*. Sinauer Associates, Incorporated.
- Crickmore, Michael A, & Mann, Richard S. 2008. The control of size in animals: insights from selector genes. *BioEssays: news and reviews in molecular, cellular and developmental biology*, **30**(9), 843–853. PMID: 18693263.
- Darzynkiewicz, Z., Crissman, H., Traganos, F., & Steinkamp, J. 1982. Cell heterogeneity during the cell cycle. *Journal of Cellular Physiology*, **113**(3), 465–474.
- Edgar, B A, & Lehner, C F. 1996. Developmental control of cell cycle regulators: a fly's perspective. *Science (New York, N.Y.)*, **274**(5293), 1646–1652. PMID: 8939845.
- Elia, Natalie, & Lippincott-Schwartz, Jennifer. 2001. Culturing MDCK Cells in Three Dimensions for Analyzing Intracellular Dynamics. In: *Current Protocols in Cell Biology*. John Wiley & Sons, Inc.
- Engler, Adam J., Sen, Shamik, Sweeney, H. Lee, & Discher, Dennis E. 2006. Matrix Elasticity Directs Stem Cell Lineage Specification. *Cell*, **126**(4), 677–689.
- Engler, Adam J, Humbert, Patrick O, Wehrle-Haller, Bernhard, & Weaver, Valerie M. 2009. Multiscale modeling of form and function. *Science (New York, N.Y.)*, **324**(5924), 208–212. PMID: 19359578.
- Escudero, Luis M, Bischoff, Marcus, & Freeman, Matthew. 2007. Myosin II regulates complex cellular arrangement and epithelial architecture in Drosophila. *Developmental cell*, **13**(5), 717–729. PMID: 17981139.
- Fidler, Isaiah J. 2003. The pathogenesis of cancer metastasis: the 'seed and soil' hypothesis revisited. *Nature reviews. Cancer*, **3**(6), 453–458. PMID: 12778135.
- Friedl, Peter, & Gilmour, Darren. 2009. Collective cell migration in morphogenesis, regeneration and cancer. *Nature reviews. Molecular cell biology*, **10**(7), 445–457. PMID: 19546857.
- Garcia-Fernandez, Beatriz, Campos, Isabel, Geiger, Jennifer, Santos, Ana C, & Jacinto, Antonio. 2009. Epithelial resealing. *The International journal of developmental biology*, **53**(8-10), 1549–1556. PMID: 19247953.
- Gaush, C R, Hard, W L, & Smith, T F. 1966. Characterization of an established line of canine kidney cells (MDCK). *Proceedings of the Society for Experimental Biology and Medicine. Society for Experimental Biology and Medicine (New York, N.Y.)*, **122**(3), 931–935. PMID: 5918973.
- George, Vinoj T, Brooks, Gavin, & Humphrey, Timothy C. 2007. Regulation of cell cycle and stress responses to hydrostatic pressure in fission yeast. *Molecular biology of the cell*, **18**(10), 4168–4179. PMID: 17699598.

- Gibson, Matthew C., Patel, Ankit B., Nagpal, Radhika, & Perrimon, Norbert. 2006. The emergence of geometric order in proliferating metazoan epithelia. *Nature*, **442**(7106), 1038–1041.
- Gibson, William T., Veldhuis, James H., Rubinstein, Boris, Cartwright, Heather N., Perrimon, Norbert, Brodland, G. Wayne, Nagpal, Radhika, & Gibson, Matthew C. 2011. Control of the Mitotic Cleavage Plane by Local Epithelial Topology. *Cell*, **144**(3), 427–438.
- Goehring, Nathan W., & Grill, Stephan W. 2013. Cell polarity: mechanochemical patterning. *Trends in Cell Biology*, **23**(2), 72–80.
- Gong, Ying, Mo, Chunhui, & Fraser, Scott E. 2004. Planar cell polarity signalling controls cell division orientation during zebrafish gastrulation. *Nature*, **430**(7000), 689–693. PMID: 15254551.
- Hagios, C, Lochter, A, & Bissell, M J. 1998. Tissue architecture: the ultimate regulator of epithelial function? *Philosophical transactions of the Royal Society of London. Series B, Biological sciences*, **353**(1370), 857–870. PMID: 9684283.
- Haigo, Saori L., & Bilder, David. 2011. Global tissue revolutions in a morphogenetic movement controlling elongation. *Science (New York, N.Y.)*, **331**(6020), 1071–1074. PMID: 21212324 PMCID: PMC3153412.
- Herant, Marc, & Dembo, Micah. 2010. Form and Function in Cell Motility: From Fibroblasts to Keratocytes. *Biophysical Journal*, **98**(8), 1408–1417.
- Hoh, J H, & Schoenenberger, C A. 1994. Surface morphology and mechanical properties of MDCK monolayers by atomic force microscopy. *Journal of cell science*, **107** (Pt 5)(May), 1105–1114. PMID: 7929621.
- Honda, Hisao. 1978. Description of cellular patterns by Dirichlet domains: The two-dimensional case. *Journal of Theoretical Biology*, **72**(3), 523–543.
- Huang, S, Brangwynne, C P, Parker, K K, & Ingber, D E. 2005. Symmetry-breaking in mammalian cell cohort migration during tissue pattern formation: role of random-walk persistence. *Cell motility and the cytoskeleton*, **61**(4), 201–213. PMID: 15986404.
- Hufnagel, Lars, Teleman, Aurelio A, Rouault, Hervé, Cohen, Stephen M, & Shraiman, Boris I. 2007. On the mechanism of wing size determination in fly development. *Proceedings of the National Academy of Sciences of the United States of America*, **104**(10), 3835–3840. PMID: 17360439.
- Ingber, Donald E. 2008. Tensegrity-based mechanosensing from macro to micro. *Progress in biophysics and molecular biology*, **97**(2-3), 163–179. PMID: 18406455.
- Jones, Chonnetia, & Chen, Ping. 2007. Planar cell polarity signaling in vertebrates. *BioEssays: news and reviews in molecular, cellular and developmental biology*, **29**(2), 120–132. PMID: 17226800.

- Kabla, Alexandre J. 2012. Collective cell migration: leadership, invasion and segregation. *Journal of The Royal Society Interface*, **9**(77), 3268–3278. PMID: 22832363.
- Khaladi, M., & Arino, O. 2000. Estimation of the Rate of Convergence of Semigroups to an Asynchronous Equilibrium. *Semigroup Forum*, **61**(2), 209–223.
- Kim, Nam-Gyun, Koh, Eunjin, Chen, Xiao, & Gumbiner, Barry M. 2011. E-cadherin mediates contact inhibition of proliferation through Hippo signaling-pathway components. *Proceedings of the National Academy of Sciences of the United States of America*, **108**(29), 11930–11935. PMID: 21730131 PMCID: PMC3141988.
- Koch, Arthur L. 1980. Does the variability of the cell cycle result from one or many chance events? , *Published online: 03 July 1980; | doi:10.1038/286080a0*, **286**(5768), 80–82.
- Lecuit, Thomas. 2010. alpha-catenin mechanosensing for adherens junctions. *Nature cell biology*, **12**(6), 522–524. PMID: 20453846.
- Lecuit, Thomas, & Goff, Loïc Le. 2007. Orchestrating size and shape during morphogenesis. *Nature*, **450**(7167), 189–192.
- Levayer, Romain, & Lecuit, Thomas. 2008. Breaking down EMT. *Nature cell biology*, **10**(7), 757–759. PMID: 18591967.
- Li, Yingzi, Naveed, Hammad, Kachalo, Sema, Xu, Lisa X., & Liang, Jie. 2012. Mechanisms of Regulating Cell Topology in Proliferating Epithelia: Impact of Division Plane, Mechanical Forces, and Cell Memory. *PLoS ONE*, **7**(8). PMID: 22912800 PMCID: PMC3422310.
- Liu, Ce. 2009. *Beyond pixels : exploring new representations and applications for motion analysis*. Thesis, Massachusetts Institute of Technology. Thesis (Ph. D.)—Massachusetts Institute of Technology, Dept. of Electrical Engineering and Computer Science, 2009.
- Marieb, Elaine N., & Mitchell, Susan. 2009. *Human Anatomy and Physiology*. 9th edn. Benjamin-Cummings Publishing Company, Subs of Addison Wesley Longman, Inc.
- Mattick, John S. 2009. Has evolution learnt how to learn? *EMBO reports*, **10**(7), 665. PMID: 19568258.
- Mayor, Roberto, & Carmona-Fontaine, Carlos. 2010. Keeping in touch with contact inhibition of locomotion. *Trends in cell biology*, **20**(6), 319–328. PMID: 20399659.
- Mazzocchi, Fulvio. 2012. Complexity and the reductionism-holism debate in systems biology. *Wiley interdisciplinary reviews. Systems biology and medicine*, **4**(5), 413–427. PMID: 22761024.
- Méchal, Marcel, & Lutzmann, Malik. 2008. The Cell Cycle: Now Live and in Color. *Cell*, **132**(3), 341–343.

- Milán, M, Campuzano, S, & García-Bellido, A. 1996. Cell cycling and patterned cell proliferation in the *Drosophila* wing during metamorphosis. *Proceedings of the National Academy of Sciences of the United States of America*, **93**(21), 11687–11692. PMID: 8876197 PMCID: PMC38119.
- Misfeldt, D S, Hamamoto, S T, & Pitelka, D R. 1976. Transepithelial transport in cell culture. *Proceedings of the National Academy of Sciences of the United States of America*, **73**(4), 1212–1216. PMID: 1063404 PMCID: PMC430232.
- Mogilner, Alex, & Keren, Kinneret. 2009. The Shape of Motile Cells. *Current Biology*, **19**(17), R762–R771.
- Montell, Denise J. 2008. Morphogenetic Cell Movements: Diversity from Modular Mechanical Properties. *Science*, **322**(5907), 1502–1505.
- Morrison, Helen, Sherman, Larry S., Legg, James, Banine, Fatima, Isacke, Clare, Haipek, Carrie A., Gutmann, David H., Ponta, Helmut, & Herrlich, Peter. 2001. The NF2 tumor suppressor gene product, merlin, mediates contact inhibition of growth through interactions with CD44. *Genes & Development*, **15**(8), 968–980.
- Nelson, Celeste M, & Bissell, Mina J. 2006. Of extracellular matrix, scaffolds, and signaling: tissue architecture regulates development, homeostasis, and cancer. *Annual review of cell and developmental biology*, **22**, 287–309. PMID: 16824016.
- Newman, Robert H., & Zhang, Jin. 2008. Fucci: Street Lights on the Road to Mitosis. *Chemistry & Biology*, **15**(2), 97–98.
- Nisticò, Paola, Bissell, Mina J, & Radisky, Derek C. 2012. Epithelial-mesenchymal transition: general principles and pathological relevance with special emphasis on the role of matrix metalloproteinases. *Cold Spring Harbor perspectives in biology*, **4**(2). PMID: 22300978.
- Nobes, C D, & Hall, A. 1999. Rho GTPases control polarity, protrusion, and adhesion during cell movement. *The Journal of cell biology*, **144**(6), 1235–1244. PMID: 10087266.
- Noble, Denis. 2011. A theory of biological relativity: no privileged level of causation. *Interface Focus*, Nov.
- Nurse, P. 2000. A long twentieth century of the cell cycle and beyond. *Cell*, **100**(1), 71–78. PMID: 10647932.
- Palsson, E, & Othmer, H G. 2000. A model for individual and collective cell movement in *Dictyostelium discoideum*. *Proceedings of the National Academy of Sciences of the United States of America*, **97**(19), 10448–10453. PMID: 10984537.
- Petitjean, L, Reffay, M, Grasland-Mongrain, E, Poujade, M, Ladoux, B, Buguin, A, & Silberzan, P. 2010. Velocity fields in a collectively migrating epithelium. *Biophysical journal*, **98**(9), 1790–1800. PMID: 20441742.
- Poujade, M., Grasland-Mongrain, E., Hertzog, A., Jouanneau, J., Chavrier, P., Ladoux, B., Buguin, A., & Silberzan, P. 2007. Collective Migration of an Epithelial

- Monolayer in Response to a Model Wound. *Proceedings of the National Academy of Sciences of the United States of America*, **104**(41), 15988–15993. ArticleType: research-article / Full publication date: Oct. 9, 2007 / Copyright © 2007 National Academy of Sciences.
- Puliafito, Alberto, Hufnagel, Lars, Neveu, Pierre, Streichan, Sebastian, Sigal, Alex, Fygenon, D. Kuchnir, & Shraiman, Boris I. 2012. Collective and single cell behavior in epithelial contact inhibition. *Proceedings of the National Academy of Sciences*, **109**(3), 739–744.
- Qu, Zhilin, Garfinkel, Alan, Weiss, James N, & Nivala, Melissa. 2011. Multi-scale modeling in biology: how to bridge the gaps between scales? *Progress in biophysics and molecular biology*, **107**(1), 21–31. PMID: 21704063.
- Rabito, C A, Tchao, R, Valentich, J, & Leighton, J. 1980. Effect of cell-substratum interaction on hemicyst formation by MDCK cells. *In vitro*, **16**(6), 461–468. PMID: 6248454.
- Ranft, Jonas, Basan, Markus, Elgeti, Jens, Joanny, Jean-François, Prost, Jacques, & Jülicher, Frank. 2010. Fluidization of tissues by cell division and apoptosis. *Proceedings of the National Academy of Sciences*, Nov.
- Ridley, Anne J. 2001. Rho GTPases and cell migration. *Journal of Cell Science*, **114**(15), 2713–2722.
- Ridley, Anne J. 2011. Life at the leading edge. *Cell*, **145**(7), 1012–1022. PMID: 21703446.
- Ridley, Anne J., Schwartz, Martin A., Burridge, Keith, Firtel, Richard A., Ginsberg, Mark H., Borisy, Gary, Parsons, J. Thomas, & Horwitz, Alan Rick. 2003. Cell Migration: Integrating Signals from Front to Back. *Science*, **302**(5651), 1704–1709.
- Rørth, Pernille. 2012. Fellow travellers: emergent properties of collective cell migration. *EMBO reports*, **13**(11), 984–991. PMID: 23059978.
- Sakaue-Sawano, Asako, Kurokawa, Hiroshi, Morimura, Toshifumi, Hanyu, Aki, Hama, Hiroshi, Osawa, Hatsuki, Kashiwagi, Saori, Fukami, Kiyoko, Miyata, Takaki, Miyoshi, Hiroyuki, Imamura, Takeshi, Ogawa, Masaharu, Masai, Hisao, & Miyawaki, Atsushi. 2008. Visualizing spatiotemporal dynamics of multicellular cell-cycle progression. *Cell*, **132**(3), 487–498. PMID: 18267078.
- Schwartz, Martin A., & Chen, Christopher S. 2013. Deconstructing Dimensionality. *Science*, **339**(6118), 402–404.
- Schwarz, Ulrich. 2004. *Forces and Elasticity in Cell Adhesion*. Habilitationsschrift am Institut für Physik und Astronomie der Mathematisch-Naturwissenschaftlichen Fakultät der Universität Potsdam.
- Shook, David, & Keller, Ray. 2003. Mechanisms, mechanics and function of epithelial-mesenchymal transitions in early development. *Mechanisms of Development*, **120**(11), 1351–1383.

- Shraiman, Boris I. 2005. Mechanical feedback as a possible regulator of tissue growth. *Proceedings of the National Academy of Sciences of the United States of America*, **102**(9), 3318–3323. PMID: 15728365.
- Sommer, C., Straehle, C., Kothe, U., & Hamprecht, F.A. 2011 (Apr.). Ilastik: Interactive learning and segmentation toolkit. *Pages 230–233 of: 2011 IEEE International Symposium on Biomedical Imaging: From Nano to Macro*.
- Strauss, Bernhard, Adams, Richard J, & Papalopulu, Nancy. 2006. A default mechanism of spindle orientation based on cell shape is sufficient to generate cell fate diversity in polarised *Xenopus* blastomeres. *Development (Cambridge, England)*, **133**(19), 3883–3893. PMID: 16943269.
- Takai, Yoshimi, Miyoshi, Jun, Ikeda, Wataru, & Ogita, Hisakazu. 2008. Nectins and nectin-like molecules: roles in contact inhibition of cell movement and proliferation. *Nature Reviews Molecular Cell Biology*, **9**(8), 603–615.
- Talia, Stefano Di, Skotheim, Jan M., Bean, James M., Siggia, Eric D., & Cross, Frederick R. 2007. The effects of molecular noise and size control on variability in the budding yeast cell cycle. *Nature*, **448**(7156), 947–951.
- Tanner, C, Frambach, D A, & Misfeldt, D S. 1983. Transepithelial transport in cell culture. A theoretical and experimental analysis of the biophysical properties of domes. *Biophysical Journal*, **43**(2), 183–190. PMID: 6616007 PMCID: PMC1329248.
- Tanner, Kandice, Mori, Hidetoshi, Mroue, Rana, Bruni-Cardoso, Alexandre, & Bissell, Mina J. 2012. Coherent angular motion in the establishment of multicellular architecture of glandular tissues. *Proceedings of the National Academy of Sciences*, Jan.
- Tanos, B, & Rodriguez-Boulan, E. 2008. The epithelial polarity program: machineries involved and their hijacking by cancer. *Oncogene*, **27**(55), 6939–6957. PMID: 19029936.
- Théry, Manuel, & Bornens, Michel. 2008. Get round and stiff for mitosis. *HFSP journal*, **2**(2), 65–71. PMID: 19404473.
- Theveneau, Eric, & Mayor, Roberto. 2010. Integrating chemotaxis and contact-inhibition during collective cell migration. *Small GTPases*, **1**(2), 113–117. PMID: 21686264 PMCID: PMC3116595.
- Theveneau, Eric, & Mayor, Roberto. 2011. Can mesenchymal cells undergo collective cell migration? *Cell Adhesion & Migration*, **5**(6), 490–498. PMID: 22274714 PMCID: PMC3277782.
- Thiery, Jean Paul, & Sleeman, Jonathan P. 2006. Complex networks orchestrate epithelial–mesenchymal transitions. *Nature Reviews Molecular Cell Biology*, **7**(2), 131–142.
- Thomas, S R, Schultz, S G, & Lever, J E. 1982. Stimulation of dome formation in MDCK kidney epithelial cultures by inducers of differentiation: dissociation from

- effects on transepithelial resistance and cyclic AMP levels. *Journal of cellular physiology*, **113**(3), 427–432. PMID: 6294127.
- Trepat, Xavier, & Fredberg, Jeffrey J. 2011. Plithotaxis and emergent dynamics in collective cellular migration. *Trends in cell biology*, **21**(11), 638–646. PMID: 21784638.
- Trepat, Xavier, Wasserman, Michael R., Angelini, Thomas E., Millet, Emil, Weitz, David A., Butler, James P., & Fredberg, Jeffrey J. 2009. Physical forces during collective cell migration. *Nature Physics*, **5**(6), 426–430.
- Wada, Ken-Ichi, Itoga, Kazuyoshi, Okano, Teruo, Yonemura, Shigenobu, & Sasaki, Hiroshi. 2011. Hippo pathway regulation by cell morphology and stress fibers. *Development (Cambridge, England)*, **138**(18), 3907–3914. PMID: 21831922.
- Walker, Sara Imari, & Davies, Paul C. W. 2013. The algorithmic origins of life. *Journal of The Royal Society Interface*, **10**(79).
- Wang, Chun-Chao, Jamal, Leen, & Janes, Kevin A. 2012. Normal morphogenesis of epithelial tissues and progression of epithelial tumors. *Wiley interdisciplinary reviews. Systems biology and medicine*, **4**(1), 51–78. PMID: 21898857.
- Weijer, Cornelis J. 2009. Collective cell migration in development. *Journal of Cell Science*, **122**(18), 3215–3223.
- Wirtz, Denis, Konstantopoulos, Konstantinos, & Searson, Peter C. 2011. The physics of cancer: the role of physical interactions and mechanical forces in metastasis. *Nature Reviews Cancer*, **11**(7), 512–522.
- Yamazaki, D., Kurisu, S., & Takenawa, T. 2009. Involvement of Rac and Rho signaling in cancer cell motility in 3D substrates. *Oncogene*, **28**(13), 1570–1583.
- Zegers, Mirjam M. P., O'Brien, Lucy E., Yu, Wei, Datta, Anirban, & Mostov, Keith E. 2003. Epithelial polarity and tubulogenesis in vitro. *Trends in Cell Biology*, **13**(4), 169–176.
- Zhao, Bin, Tumaneng, Karen, & Guan, Kun-Liang. 2011. The Hippo pathway in organ size control, tissue regeneration and stem cell self-renewal. *Nature Cell Biology*, **13**(8), 877–883.

List of Figures

0.1. Biological relativity	11
1.1. Epithelial tissues	14
1.2. Tumorigenesis via EMT	15
1.3. MDCK cells in low and high density	17
1.4. The cell cycle and its checkpoints	19
1.5. Contact inhibition of proliferation	21
1.6. Cell area dependence of division times	22
1.7. Hippo signaling pathway	22
1.8. Oriented cell divisions	24
1.9. Structure of a motile cell	28
1.10. Epithelial rotations	30
1.11. Mechanical feedback as a growth regulator	31
1.12. Vertex model	33
2.1. Cell number and density	37
2.2. Cell cycle distributions	38
2.3. Experimental age distributions	39
2.4. Gauss fit	41
2.5. Modeled age distributions	41
2.6. Asymptotic stationary age distribution	42
2.7. Cell pair symmetries	43
3.1. Relative motility and proliferation	45
3.2. Angular velocity and mitosis density	46
3.3. Summary of angular velocity and mitosis density	47
3.4. Mother / daughters migration correlation	48

3.5. Division axis orientation	49
5.1. Fucci marker	55
5.2. Trainable segmentation	57
5.3. Single cell tracks	58
A.1. Medium sensitivity of cellular motility	59
A.2. Density heterogeneities	60
A.3. Wellsize-dependent proliferation behaviour	61

Nomenclature

AFM	Atomic force microscopy
cAMP	Cyclic adenosine monophosphate
CCC	Cell cycle correlations
CCD	Cell cycle periods distribution
CDK	Cyclin-dependent kinase
CIP	Contact inhibition of proliferation
CV	Coefficient of variation
Dpp	Decapentaplegic
ECM	Extracellular matrix
EMT	Epithelial-mesenchymal transition
Fucci	Fluorescent ubiquitination-based cell cycle marker
MDCK	Madin-Darby Canine Kidney
MET	Mesenchymal-epithelial transition
MMPs	Matrix metalloproteinases
PCP	Planar cell polarity
PDMS	Polydimethylsiloxane
YAP	Yes-associated protein

Acknowledgements

First of all I like to thank Lars Hufnagel for having me in his research group.

I am also grateful to the other members of my thesis advisory committee - Ulrich Schwarz, Darren Gilmour, and Stefano De Renzis - for most useful recommendations at critical checkpoints of my time as a PhD student at the European Molecular Biology Laboratory (EMBL).

I want to thank Tatjana Schneidt and, previously, Daniela Holzer for keeping our cell cultures alive, the experiments running, and the lab organised.

Also, I like to thank all other group members, especially Sebastian Streichan and Christian Hoerner, my predoc predecessors and first contact persons for issues concerning physics and biology, respectively. Further, I thank Stefan Günther, Timothy Saunders, and Uroš Kržič for support based on their postdoctoral experience. Special thanks to Christian Hoerner for most proper proofreading of my work.

In addition, I like to thank Katarzyna Tarnawska, Beat Rupp and François Nédélec for their support of an additional experiment based on micropatterned substrates, though this was not realised in the end due to a lack of time.

Particularly, I want to thank Halldór Stefánsson and the EMBL Science and Society committee for letting me participate in exciting interdisciplinary events and for giving me the opportunity to meet extraordinary people.

Also, I like to thank my musical colleagues for pleasant hours of playing together: Claude Antony for the wonderful chamber music and Marcus Heisler for propelling the EMBL Jam Club. Special thanks to Tobias Just and the EMBL choir for common performances.

I want to thank my partner Caroline Zöllner for being tolerant in the tough times and always motivating a good work-life balance.

Last but not least I thank my parents and sisters for supporting all my plans.